



Reviews of High-Longevity Aqueous Zinc Metal Batteries Achieved by Programmable Interface Architectures

Bixian Chen, Xiaomin Cheng, Haifeng Yang, Teng Li, Jing Dong, Yidong Miao, Yongzheng Zhang , Qingbo Xiao*, Qinghua Guan, Jing Zhang, Yunjian Liu*, Hongzhen Lin*, and Jian Wang* 

Aqueous zinc metal batteries (AZMBs) are considered ideal ones for next-generation energy storage devices due to their high theoretical specific capacity and intrinsic safety. However, uncontrollable zinc dendrite growth, hydrogen evolution reaction (HER), and interface corrosion prohibit the commercialization of AZMBs. The deposition behaviors of $\text{Zn}^{2+}/\text{Zn}^0$ on metallic Zn surface can be effectively regulated by constructing artificial interphase layers (AILs) to control desolvation and ion/atom flux. In this work, the intrinsic mechanism and interface failure of Zn^{2+} electrodeposition behaviors are initially revealed, providing a theoretical basis for interface issues. To address these problems, the design strategies from carbon materials, zincophilic alloys, and inorganic/organic compound layers provide an in-depth analysis of the relationship between material structure and performance, establishing a theoretical foundation for the development of programmable interface architecture. In light of practical application requirements, the future direction is envisioned and pioneered, aiming to promote the practical application process of AZMBs.

1. Introduction


Considering that the consumption of traditional fossil fuels is unable to meet the long-term global energy requirements, the advancement of clean and renewable energy resources (such as solar, wind, and tidal energy) has experienced exponential growth in recent years.^[1–3] The development of energy storage systems has confronted significant chal-

lenges in safety, lifespan, and energy density.^[4–9] Since their commercialization in 1991, lithium-ion batteries (LIBs) have become the most advanced and widely commercial battery-based energy storage solution in modern society. However, current LIBs are constrained by the flammability of their electrolytes, environmental pollution, and high costs, falling short of sustainable development requirements.^[10–19] Hence, researchers have focused on developing battery systems with anode materials that are more abundant and cost-effective than lithium. Multivalent metal battery systems (e.g., Ca,^[20] Mg,^[21] Al,^[22] Zn^[23]) have emerged as a focal point of research. The zinc anode stands out because of its high theoretical capacities (820 mAh g^{-1} and 5855 mAh cm^{-3}), low redox potential (-0.76 V vs. SHE), and exceptional chemical stability.^[24–26] Besides, aqueous electrolytes based on water solvent are promising for developing advanced energy storage devices due to their inherent safety. There is an increasing

research focus on rechargeable aqueous zinc metal batteries (AZMBs) that use neutral or mildly acidic aqueous electrolytes.

Despite the significant application potential of AZMBs, several challenges are obvious as follows: 1) the limited active sites of cathode materials and the structural collapse which will restrict the battery capacities;^[27–29] 2) the narrow working potential window and the electrochemical instability of aqueous electrolytes limit the application

B. Chen, H. Yang, T. Li, Prof. Y. Liu
School of Materials Science and Engineering, Jiangsu University, Zhenjiang 212013, China
E-mail: lyjian122331@ujs.edu.cn
B. Chen, Dr. X. Cheng, H. Yang, J. Dong, Q. Guan, Prof. H. Lin
i-Lab & CAS Key Laboratory of Nanophotonic Materials and Devices, Suzhou Institute of Nano-Tech and Nano-Bionics, Chinese Academy of Sciences, Suzhou 215123, China
E-mail: hzlin2010@sinano.ac.cn
Dr. J. Wang
Helmholtz Institute Ulm (HIU), Ulm D89081, Germany
Karlsruhe Institute of Technology (KIT), Karlsruhe D76021, Germany
E-mail: wangjian2014@sinano.ac.cn; jian.wang@kit.edu
Dr. Q. Xiao
Institute of Agricultural Resources and Environment, Jiangsu Academy of Agricultural Sciences, Nanjing 210014, China
E-mail: qbxxiao@jaas.ac.cn

Dr. Y. Miao
School of Materials and Chemical Engineering, Xuzhou University of Technology, Xuzhou 221018, China
Dr. Y. Zhang
State Key Laboratory of Chemical Engineering, East China University of Science and Technology, Shanghai 200237, China
Dr. J. Zhang
School of Materials Science and Engineering, Xi'an University of Technology, Xi'an 710048, China
Dr. X. Cheng
Guangdong Institute of Semiconductor Micro-Nano Manufacturing Technology, Guangdong 518103, China
 The ORCID identification number(s) for the author(s) of this article can be found under <https://doi.org/10.1002/eem2.70176>.

DOI: 10.1002/eem2.70176

under high-voltage application;^[30] 3) due to uncontrollable zinc dendrite growth, hydrogen evolution reaction (HER) and interface corrosion at the anodes result in poor battery reversibility and low zinc utilization.^[3,31,32] It is noteworthy that a high-performance zinc anode is essential to guarantee the excellent cycling stability and lifespan of AZMBs. Consequently, research focusing on developing stable zinc anodes is essential for the commercialization of AZMBs.^[33,34]

To date, researchers have explored various strategies to stabilize the zinc anode, including electrolyte engineering,^[35,36] separator modification,^[37–40] and constructing artificial interphase layers (AILs).^[41–44] Research in electrolyte engineering primarily focuses on adding functional additives to traditional electrolytes.^[45] These strategies, such as constructing functional electrolytes,^[46–49] organic cosolvent engineering,^[50,51] and solid-state electrolytes aim at enhancing the compatibility between zinc metal anodes and electrolyte interface. However, the relatively weak electrostatic shielding effect between these additives and the water molecules surrounding Zn^{2+} is insufficient to effectively exclude water from the inner Helmholtz plane. This leads to continuous HER and severe deterioration of AZMBs.^[52,53] At the same time, this strategy may increase electrolyte viscosity, leading to increased polarization and reduced plating/stripping efficiency, along with unsatisfactory zinc utilization.^[54] The separator modification strategy can homogenize the electric field, reducing the growth of dendrites due to the uneven nucleation sites and inhibiting the growth of zinc dendrites to a certain extent.^[55] However, the development of the separator needs to address the issues of cost and scalability, as these present significant challenges for the large-scale application of AZMBs. As shown in **Figure 1**, constructing an AIL between the zinc anode and the electrolyte has proven to be a simple and effective method.^[56,57] AILs provide several advantages. On the one hand, these AILs act as a barrier, reducing contact between the zinc anode and the aqueous electrolyte, thereby effectively reducing side reactions. On the other hand, they can also introduce nucleation sites and regulate the electric field distribution, guiding uniform Zn^{2+} deposition and inhibiting dendrite growth.^[58] In addition, AILs can be prepared for scaling up by simple processes such as scraping and spraying with great commercialization prospects.

In recent years, a series of materials, including carbon materials, zincophilic alloys, and inorganic/organic compounds, have been widely used as AILs to protect zinc anodes. For instance, the Sn@Zn anode exhibited a cycle lifespan of 1000 h at 0.5 mA cm^{-2} , but showed a significant increase in voltage hysteresis during cycling.^[58] Similarly, the PVA@Zn electrode developed by Chen et al.^[59] achieved $\approx 350 \text{ h}$ at 5 mA cm^{-2} . However, a higher overpotential compared to bare Zn was observed. It is essential to recognize that the reported materials for zinc anode protection still have significant limitations.^[60] Owing to intrinsic material properties, single-component materials are often restricted by their inherent material deficiencies, limiting their ability to address various issues faced by zinc anodes.^[61] This limitation prevents current AIL construction strategies from achieving the practical requirements of high depth of discharge (DOD), high energy density,^[62] long cycle lifespan, and superior cycling stability.^[63] Consequently, future research will necessarily focus on the design of composite coatings with multi-component formulations, multiscale structures, and multifunctional capabilities. Although several composite coatings have been reported to date, the strategies for material selection remain insufficiently systematic and lack clear design principles and methodologies. Therefore, clarifying the regulatory mechanism of different material



Bixian Chen is a jointly trained student between Jiangsu University and the Suzhou Institute of Nano-Tech and Nano-Bionics, Chinese Academy of Sciences. His research focuses on the development and application of aqueous zinc metal batteries.



Dr. Qingbo Xiao is currently an associate researcher at Institute of Agricultural Resources and Environment, Jiangsu Academy of Agricultural Sciences (JAAS). He majors in developing novel technologies for renewable energy utilizations such as secondary batteries and solar-driven water remediation as well as

Operando characterizations.



Prof. Yunjian Liu is a doctoral supervisor and the Dean of the School of Materials Science and Engineering at Jiangsu University. He serves as a member of the Physical Chemistry Committee and the New Energy Materials Development Committee of the Chinese Nonferrous Metals Society. His research

focuses on the key materials of novel lithium/zinc/sodium-ion batteries, new energy materials and materials electrochemistry, as well as value-added metallurgy of nonferrous metals.



Prof. Hongzhen Lin is a senior researcher at *i*-lab of Suzhou Institute of Nano-Tech and Nano-bionics, Chinese Academy of Sciences, and University of Science and Technology of China. He majors in developing high energy density lithium metal-based energy storage systems with catalytic functionalities

and their in situ interfacial nonlinear spectroscopy characterization.



Dr. Jian Wang is currently a research fellow supported by Alexander von Humboldt foundation in Helmholtz Institute Ulm (HIU) and Karlsruhe Institute of Technology (KIT). His research interests focus on the applications of catalysis in modulating electrochemical kinetics of secondary batteries ('Catalysis-in-Batteries') and the exploration of in situ characterizations for probing interface mechanisms.

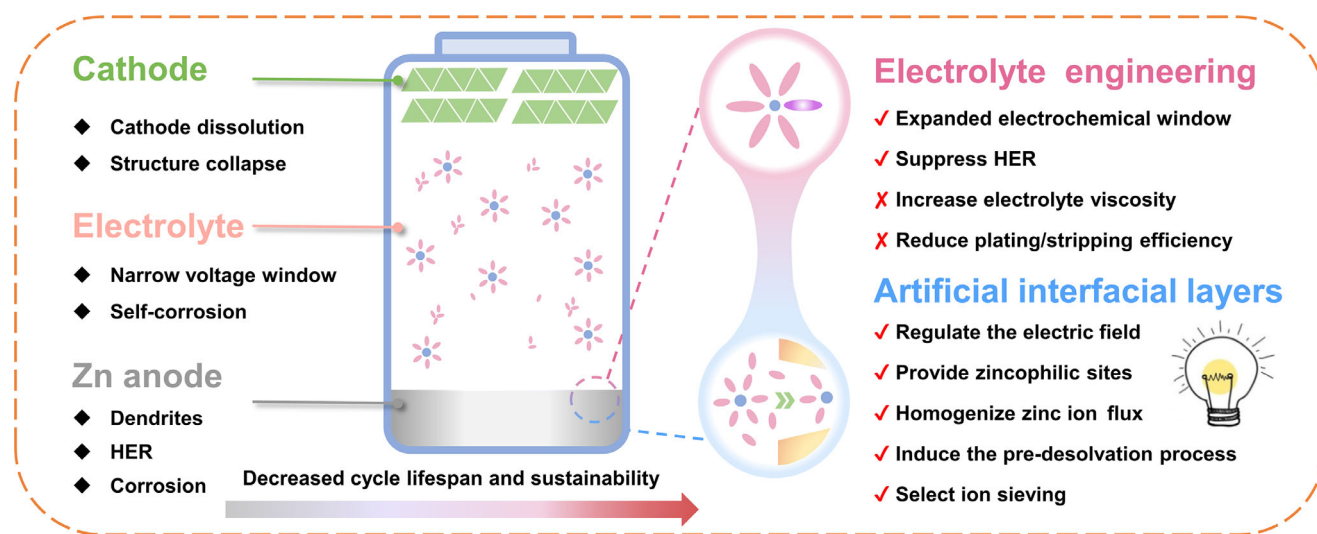


Figure 1. Schematic illustration of the challenges in aqueous zinc-metal batteries and the comparison between electrolyte engineering and artificial interfacial layers applied in prohibiting Zn dendrite formation.

systems at the interface of zinc anodes, combined with analyzing the constitutive relationship between the structural properties for the deposition behavior of zinc ions, would be beneficial for providing theoretical guidance for the design of novel composite materials and enhancing the electrochemical performance of AZMBs.

This work systematically summarizes the design principles and research progress of AILs for zinc plating, and clarifies the possible development paths for constructing high-performance AZMBs. Specifically, the fundamental mechanism of zinc anode failure is initially analyzed. Subsequently, the construction strategies for various AILs and their performance optimization methods are comprehensively reviewed. Finally, the future development of AILs toward high-performance AZMBs is discussed prospectively.

2. Principles of Zinc-Ion Deposition and Failure Mechanisms of Zinc Anode

2.1. Principles of Zinc-Ion Deposition

Similar to LIBs, AZMBs comprise three components: 1) a zinc metal anode, 2) an aqueous electrolyte, and 3) a cathode.^[64] During the discharging process, the Zn metal anode undergoes oxidation to zinc ions, releasing electrons. During the charging process, zinc ions are reversibly redeposited onto the Zn anode from the cathode. The conversion reaction of Zn during deposition and dissolution is demonstrated in Equation (1):



The electrochemical deposition process of zinc ions on the anode is illustrated in **Figure 2a**. First, the $[\text{Zn}(\text{H}_2\text{O})_6]^{2+}$ migrates toward the electrode surface from the solution under an electric field. As $[\text{Zn}(\text{H}_2\text{O})_6]^{2+}$ approaches the Helmholtz layer, it sequentially releases the hydration shells to yield a bare Zn^{2+} for subsequent reduction. After that, the desolvated zinc ions diffuse to the electrode surface, transfer electrons, and are reduced to metallic zinc atoms. The electro-deposited zinc atoms experience surface self-diffusion, gradually accumulating

into stable two-dimensional nuclei. Upon reaching a critical potential, the zinc nuclei grow and sequentially undergo the morphological evolution of electrodeposition, progressing through nucleation, planar growth, and ultimately bulk zinc crystal accumulation. As the process proceeds, the new crystal layer grows on different crystal planes, resulting in a macroscopic deposited crystal structure.

The crystal orientation of the electrode induces the growth direction of the newly deposited metal, which means that the crystallographic heterogeneity of the metal electrode translates into inhomogeneity of the deposited metal morphology. Typically, zinc crystals possess a hexagonal close-packed (hcp) structure, predominantly exhibiting the Zn(002), Zn(100), and Zn(101) planes during the zinc deposition process. These crystallographic planes display distinctly different atomic arrangements and surface properties. The Zn(002) crystal plane features an orderly atomic arrangement and a smooth surface, characterized by relatively uniform equipotential surfaces and a more compact structure.^[65] In contrast, the atomic arrangements on the Zn(100) and Zn(101) planes are more wavy and irregular. When Zn deposits on the Zn(002) plane, the deposited Zn tends to grow at a small angle (0° – 30° relative to the substrate), inducing horizontal Zn deposition.^[66] This deposition behavior provides favorable sites for subsequent flat Zn growth. In contrast, when Zn deposits on the Zn(100) and Zn(101) planes, the deposited Zn tends to grow at a large angle (70° – 90° relative to the substrate), forming Zn nanosheets. Since Zn stripping preferentially occurs from the bottom, the top portion of these nanosheets can easily evolve into “dead Zn.” Therefore, Zn electrodes with a higher proportion of exposed (002) planes are considered an effective strategy for achieving planar and dendrite-free Zn deposition.^[67]

2.2. Failure Mechanisms of Zinc Anode

2.2.1. Zn Dendrite Formation

Dendrite growth is a significant challenge faced by the majority of metal-ion batteries, including those using Li and Zn.^[68–71] It is closely related to the inhomogeneous distribution of the interfacial electric field and ion flux on the anode. In order to reduce the energy barrier for

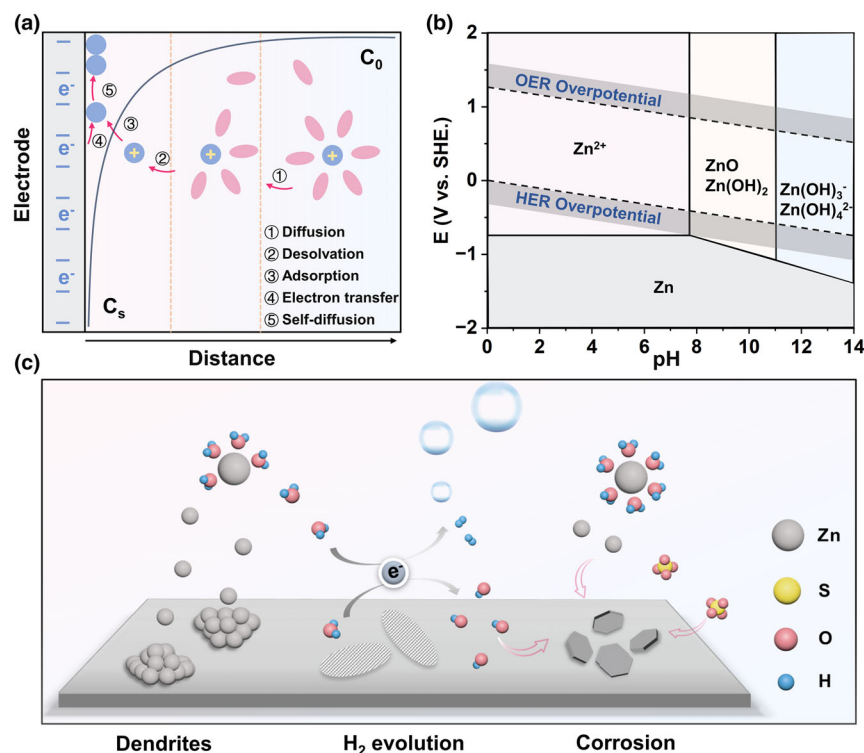


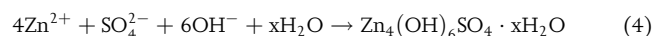
Figure 2. a) Schematic diagram of the gradual step in Zn deposition process, C_0 and C_s are the concentration of Zn^{2+} cations in the bulk electrolyte or at the interface, respectively. b) The Pourbaix diagram of Zn in aqueous electrolyte. c) Schematic illustration of challenges in Zn anodes from sluggish desolvation, HER evolution to dendrite formation.

nucleation, crystals tend to nucleate preferentially in regions with the lowest energy. The inherent lattice defects and impurities of commercial zinc foils on the surface provide favorable energy sites for the heterogeneous nucleation of zinc atoms. As a result, the initial deposition behavior of Zn^{2+} is inhomogeneous and regions of preferential nucleation will rapidly grow and form protrusions.^[72] In addition, the electric field strength at the protrusion site is higher, which attracts more Zn^{2+} aggregation and thereby accelerates Zn deposition. This phenomenon is known as the “tip effect.”^[73] Furthermore, the high $[Zn(H_2O)_6]^{2+}$ desolvation energy barrier causes the slow Zn^{2+} migration kinetics, while the fast electron coupling reaction of Zn^{2+} at the electrode surface rapidly depletes desolvated Zn^{2+} . The mismatch between the migration rate of Zn^{2+} in the electrolyte and the deposition rate on the electrode surface triggers interfacial concentration polarization, thereby disturbing the electric field distribution of the electric double layer. As a result, energy-driven nucleation and slow $[Zn(H_2O)_6]^{2+}$ desolvation kinetics result in the inhomogeneous deposition of Zn^{2+} on the electrode surface, promoting continuous dendritic zinc growth. In addition, the fracture and shedding of dendrites during the cycling process also form irreversible “dead zinc,” which significantly reduces zinc utilization and severely affects electrochemical performance.

2.2.2. HER and Corrosion Reaction

In AZMBs, interfacial side reactions are closely related to the non-ideal behavior of water molecules at the electrode/electrolyte interface. The

ionic conductivity of aqueous electrolytes is two orders of magnitude higher than that of organic electrolytes, while also ensuring the economic viability and inherent safety of AZMBs. However, its presence also poses significant challenges. Based on thermodynamic Pourbaix analysis (Figure 2b), it is indicated that HER has a more significant thermodynamic advantage in a weakly acidic environment.^[74] The lower hydrogen adsorption energy on the zinc anode surface and the barrier effect of the zinc oxide passivation layer effectively suppress the HER rate. However, this does not mean that HER was eliminated in AZMBs. Notably, the O-H bond strength of the ligand water molecules in $[Zn(H_2O)_6]^{2+}$ is significantly weakened compared with free water.^[75] This ligand-induced distortion of the electron cloud provides an activation pathway for the dissociation of water molecules, thereby enhancing the likelihood of HER occurrence. The continued occurrence of HER has several unfavorable effects. First, the HER will compete with the electroreduction of zinc ions, reducing the output power of the battery. Secondly, the formation of gaseous H_2 will alter the pressure distribution inside the battery, potentially resulting in swelling or mechanical failure. Finally, the decomposition of activated water will also generate a large amount of OH^- , leading to a local pH increase and the formation of corrosive passivation products, such as zinc hydroxide and alkaline zinc sulfate $(Zn(OH)_2, Zn_4(OH)_6SO_4 \cdot xH_2O)$.^[76] The specific reactions are as follows:



Compared with the dense protective solid electrolyte interphase (SEI) in LIB systems, the porous byproduct layer formed on the surface of the zinc anode not only fails to inhibit interfacial corrosion effectively but also increases the charge transfer impedance at the electrode/electrolyte interface. This byproduct layer is formed at the expense of depleting the active zinc, significantly reducing the coulombic efficiency (CE) and exacerbating dendrite growth (Figure 2c).^[75]

3. Designs and Structures for AIL

The key to stabilizing zinc metal anodes lies in the simultaneous regulation of Zn^{2+} transport kinetics and thermodynamic reduction of active water decomposition. From the view of electrochemical kinetics, first of all, optimizing the distribution of the electric field at the electrode/electrolyte interface can alleviate the “tip effect” and promote the uniform distribution of the Zn^{2+} flux. Secondly, enhancing the affinity of the substrate for Zn^{2+}/Zn^0 and introducing nucleation sites

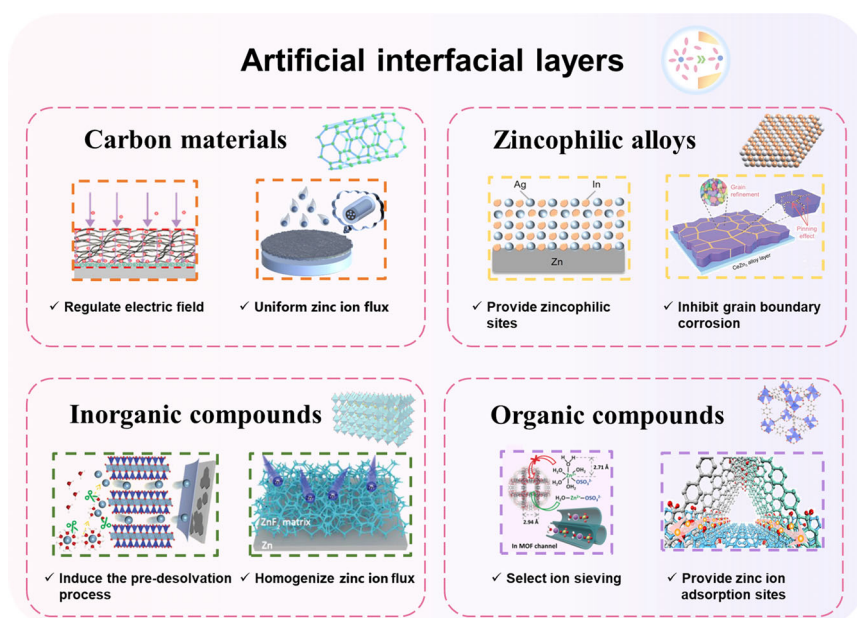


Figure 3. Artificial interphase layer with different coating materials for Zn anodes.

can create a favorable environment for zinc nucleation. In addition, the migration path of Zn^{2+} can be restricted by physically restricting the domain, driving the orderly deposition of Zn^{2+} from top to bottom along the channel instead of random deposition. From a thermodynamic point of view, HER and corrosion reactions can be effectively suppressed by modulating the solvated sheath structure of hydrated Zn^{2+} or reducing the activity of interfacial water molecules. As shown in **Figure 3**, the representative methods for modulating Zn^{2+} deposition in each category of materials are summarized. In this section, we critically analyze the mechanisms of various types of materials in constructing AILs, detailing their main functions and providing a comparative analysis of overall performance in Tables 1–4.

3.1. Carbon Materials

Balancing electron conduction and ion transport efficiencies is crucial for achieving stable zinc anode deposition. Poor solid–solid interface contact can lead to the blockage of electron transport, which in turn triggers the inhomogeneous Zn^{2+} deposition. Hence, constructing a conductive interface can effectively regulate the distribution of the electric field and improve the uniformity of the Zn flux distribution. Carbon materials show unique advantages in the field of metal anode battery protection due to their excellent electrical conductivity, high specific surface area, and stable chemical properties.^[77–79] On the one hand, the high electrical conductivity of carbon materials can promote the uniform distribution of interfacial charge and alleviate the electric field distortion. On the other hand, the high specific surface area of carbon materials introduces abundant functional groups, which serve as effective Zn^{2+} adsorption sites and regulate nucleation behavior. In addition, carbon materials possess outstanding mechanical properties that effectively suppress the risk of zinc dendrite penetration through separators. These unique characteristics make carbon materials highly promising candidates for constructing AILs in energy storage systems.^[80,81] According to the dimensional

classification, carbon materials used in AZMBs are categorized as one-dimensional (1D) carbon materials, two-dimensional (2D) carbon materials, and three-dimensional (3D) carbon materials.

3.1.1. 1D Carbon Materials

Carbon nanotubes (CNTs) are a typical 1D carbon material, consisting of a honeycomb network of hexagonal sp^2 hybridized carbon atoms.^[82] This structure endows CNTs with excellent electrical conductivity, high specific surface area, and remarkable mechanical stability. Dong et al. employed a freestanding, highly flexible, and conductive CNT scaffold to stabilize the zinc anode by regulating Zn^{2+} deposition sites through the porous framework of the scaffold.^[83] Additionally, the highly conductive CNT network has been shown to homogenize the electric field, thereby optimizing zinc plating/stripping behavior. Li et al. successfully designed a CNT coating.^[84] The CNT network was designed to incorporate a foam structure

with high porosity, created through a hydrophilic treatment. This treatment enables the effective transport of aqueous electrolytes and facilitates dendrite-free Zn deposition at high current densities (**Figure 4a**). Electrochemical impedance spectra (EIS) analysis revealed a novel small semicircular feature in the high-frequency region of the CNT-Zn system (**Figure 4b**), indicating that the interfacial process exhibits capacitive properties that promote the accumulation of Zn^{2+} and electrons. This observation is further confirmed and observed in cyclic voltammetry (CV) tests (**Figure 4c**). Electron transfer at the CNT-Zn interface was indicated by 3D charge density difference (CDD) maps (**Figure 4d**). Concurrently, the 2D CDD contour plot also confirmed that CNT facilitated electron enrichment on the metallic zinc side (**Figure 4e**). The strong adsorption of Zn^{2+} at the CNT-Zn interface leads to the formation of an enrichment layer composed of adhesive Zn^{2+} carriers, which enhances zincophilicity and facilitates the preferential growth of zinc along the (002) crystal plane.

Another commonly used carbon material, carbon nanofibers (CNF), has also been used as AILs to protect zinc anodes. Chen et al. employed an electrostatic spinning method to prepare CNF, achieving stable cycling at a 60% DOD.^[85] In addition, phosphorus-functionalized multichannel carbon interlayer (PMCCI) was developed by Shi et al., which achieved dual regulation of zinc deposition kinetics through multiscale structural design.^[86] Scanning electron microscopy (SEM) analysis revealed that PMCCI exhibits a micrometer-scale, three-dimensional crosslinked network structure, with its porous channels providing a sufficient spatial buffer for Zn deposition (**Figure 4f**). X-ray photoelectron spectroscopy (XPS) further revealed that the material surface is uniformly distributed with zincophilic functional groups such as P-C (284.6 eV) and P=O (532.1 eV), which provide abundant nucleation sites for Zn^{2+} deposition (**Figure 4g**). This synergistic effect of the porous mesh channel structure and the zincophilic functional groups enabled the PMCCI@Zn symmetric cell to exhibit an extremely low nucleation overpotential (**Figure 4h**) and achieve an ultra-long cycling life of 3300 h at a current density of 2 mA cm^{-2} .

Table 1. Summary of preparing methods and battery performances of Zn anode protected by AIL affording carbon materials.

AIL materials	Main function	Average CE [mA cm^{-2} , mAh cm^{-2}]	Cycling lifespan [mA cm^{-2} , mAh cm^{-2}]	References
CNT	Homogenizing electric field distribution		400 h (1, 1)	[83]
CNT	Homogenize electric field distribution	400 cycles, 99.4% (1, 1)	1850 h (2, 1)	[84]
CNF	Improve hydrophilicity	126 cycles, 98.3% (0.5, 0.5)	200 h (2, 2)	[85]
PMCCI	Offer nucleation sites	300 cycles, 99.4% (2, 1)	DOD = 40% 3300 h (2, 1)	[86]
rGO	Reduce volume change	–	300 h (1, 1)	[90]
Zn/rGO@CC	Homogenize electric field distribution and Zn^{2+} flux	–	980 h (1, 1)	[91]
NGO	Homogenize electric field distribution and offer nucleation sites	–	500 h (1, 1)	[92]
NGO	Guide Zn (002) growth	–	1200 h (1, 1)	[93]
NOC	Facilitate desolvation process.	800 cycles, 99.5% (10, 1)	136 h (30, 30)	[94]
Zn-VSGDY	Act as ion-oriented channels	200 cycles, over 99% (1, 0.5)	DOD \approx 63% 600 h (0.1, 0.1)	[96]
3F-GDY	Homogeneous Zn deposition	–	–	[97]
MAX (Ti_3AlC_2)	Fast transport of ion flux	–	800 h (0.2, 0.2)	[99]
SAFe@MXene	Promote Zn^{2+} desolvation and diffusion	100 cycles, 99.8% (1, 1)	1000 h (1, 1)	[100]
$\text{g-C}_3\text{N}_4$	Homogenize the Zn^{2+} flux	100 cycles, 97.6% (0.5, 0.5)	1000 h (1, 1)	[104]
PCN	Weak the water- Zn^{2+} interaction	300 cycles, 99.9% (3, 3)	2000 h (1, 1)	[103]
Cu-Ps/EG	Homogenizing electric field distribution	300 cycles, 95% (1, 1)	3000 h (5, 5)	[105]
CF-G-Cu NPs	Enhance interfacial	300 cycles, 95% (1, 1)	3000 h (5, 5)	[106]
CEG	Offer nucleation sites Promote Zn^{2+} desolvation and diffusion	–	820 h (1, 0.5)	[107]

Table 2. Summary of preparing methods and battery performances of Zn anode protected by AIL affording zincophilic alloys.

AIL materials	Main function	Average CE [mA cm^{-2} , mAh cm^{-2}]	Cycling lifespan [mA cm^{-2} , mAh cm^{-2}]	References
Au	Offer nucleation sites	60 cycles, 97.08% (0.5, 0.5)	2000 h (0.25, 0.05)	[111]
Ag	Offer nucleation sites	–	350 h (1, 1)	[112]
Ag-In	Guide uniform nucleation	1400 cycles, 99.8% (1, 0.5)	8000 h (1, 0.5)	[113]
$\text{Zn}_{88}\text{Al}_{12}$	Electrostatic shield	300 cycles, 99.4% (2, 1)	2000 h (0.5)	[114]
Pb	Enhance the HER overpotential	370 cycles, 99.0% (5, 2.5)	400 h (4, 0.5)	[115]
Bi	Guide Zn (002) growth	1400 cycles, 99.8% (2, 1)	1000 h (1.2, 0.6)	[116]
Ti	Inhibit intergranular corrosion	4000 cycles, 99.6% (5, 1)	1100 h (2, 2)	[110]
Ce	Inhibit intergranular corrosion	600 cycles, 99.8% (5, 1)	Over 4000 h (2, 2)	[118]
Cu-rich surface	Guide Zn (101) growth	1300 cycles, 99.72% (5, 1)	3600 h (5, 1)	[119]

3.1.2. 2D Carbon Materials

Graphene, a remarkable 2D carbon material, has found widespread application in energy storage devices due to its exceptional electrical conductivity, large specific surface area, and strong mechanical stability.^[87–89] The excellent electronic conductivity of graphene facilitates the rapid nucleation and growth of Zn^{2+} , thereby enabling uniform zinc deposition. Its ideal 2D structure and versatile assembly capabilities make it well-suited to serve as the principal framework for metal anodes, thereby effectively reducing volumetric fluctuations during charge and discharge cycles. The construction of zincophilic functional groups has been demonstrated to optimize ion fluxes, promote uniform nucleation of metal ions, and inhibit dendritic growth. At present, substantial research has been dedicated to employing

graphene-based materials to construct dendrite-free Zn anode coatings. Xia et al. conducted a spontaneous reduction reaction to assemble layer-by-layer structured reduced graphene oxide (rGO) on the surface of zinc foils.^[90] Zn can be deposited either on the surface of the rGO or on the inner surfaces of the layers during the plating/stripping processes, which has been shown to reduce the local current density (**Figure 5a**) significantly. In addition, Wang et al. co-assembled Zn nanosheets and rGO onto carbon cloth (CC) by co-electrophoresis to form a Zn/rGO@CC composite anode.^[91] The results of the electric field distribution simulation show that the Zn@CC electrode exhibits an inhomogeneous electric field distribution, with the maximum electric field intensity occurring near protrusion regions on the electrode surface. This localized high electric field intensity attracts zinc ions to accumulate at the protrusion tips, leading to inhomogeneous zinc

Table 3. Summary of preparing methods and battery performances of Zn anode protected by AIL affording inorganic compounds.

AIL materials	Main function	Average CE [mA cm ⁻² , mAh cm ⁻²]	Cycling lifespan [mA cm ⁻² , mAh cm ⁻²]	References
CaCO ₃	Optimize transport channels	–	836 h (0.25, 0.05)	[121]
ZrO ₂	Induce Maxwell-Wagner polarization	230 cycles, 99.36% (5, 1)	2100 h (5, 1)	[122]
Nb ₂ O ₅	Induce Maxwell-Wagner polarization	100 cycles, 98.01% (1, 0.5)	1000 h (1, 0.5)	[123]
BaTiO ₃	Induce Maxwell-Wagner polarization	–	2000 h (1, 1)	[124]
t-KTN	Induce Maxwell-Wagner polarization	200 cycles, 97.6% (2, 1)	1200 h (1, 1)	[127]
BaTiO ₃	Enhance desolvation and diffusion kinetics	1000 cycles, 99.9% (5, 1)	600 h (10, 3)	[129]
Zn(NbO ₃) ₂	Enhance desolvation and diffusion kinetics	1200 cycles, 99.54% (1, 1)	1000 h (10, 10) DOD = 34.1%	[130]
Zn ₂ SiO ₄	Enhance desolvation and diffusion kinetics	600 cycles, 99.8% (2, 1)	3300 h (0.5, 0.5)	[131]
ZnF ₂	Redistribute the Zn ²⁺ flux and reduce the desolvation active energy	500 cycles, 99.8% (5, 1)	800 h (1, 1)	[132]
ZnF ₂ -In	Promote Zn ²⁺ desolvation and diffusion	100 cycles, 99.8% (1, 1)	4200 h (1, 1)	[133]
ZnS	Isolate Zn/H ₂ O	200 cycles, 99.2% (2, 1)	1100 h (2, 2)	[135]
ZnSe	Optimize transport channels	–	1700 h (1, 0.5)	[136]
TiN	Inhibit side reaction	–	2300 h (1, 1)	[137]

Table 4. Summary of preparing methods and battery performances of Zn anode protected by AIL affording organic compounds.

AIL materials	Main function	Average CE [mA cm ⁻² , mAh cm ⁻²]	Cycling lifespan [mA cm ⁻² , mAh cm ⁻²]	References
PA	Harmonize Zn ²⁺ migration	300 cycles, 95.12% (0.4, 0.4)	8000 h (0.5, 0.25)	[141]
PVB	Promote Zn ²⁺ desolvation and diffusion	100 cycles, 99.4% (4, 2)	2200 h (0.5, 0.5)	[142]
PVA	Guide Zn (002) growth	500 cycles, over 99% (5, 1)	2200 h (1, 1)	[59]
PANZ	Improve hydrophilicity	770 cycles, 99.8% (1, 1)	1145 h (1, 1)	[143]
PMMA	Optimize transport channels	1000 cycles, 99.8% (1, 1)	4000 h (1, 1)	[144]
ZIF-7	Select ion sieving	–	3000 h (0.5, 0.5)	[146]
ZIF-8	Optimize transport channels	300 cycles, 99.4% (5, 5)	1200 h (2, 1)	[147]
UiO-66-(COOH) ₂	Enhance desolvation and diffusion kinetics	200 cycles, 99.4% (1, 1)	2800 h (2, 2)	[148]
Zn-AAAn-COF	Uniform Zn ²⁺ flux	600 cycles, 98.7% (2, 1)	300 h (20, 1)	[152]
SPCOF	Reduce the surface energy of the nanochannels	1000 cycles, 99.5% (1, 1)	5000 h (1, 1)	[153]
PI-DT-COF	Promote Zn ²⁺ diffusion	160 cycles, 99% (10, 1)	200 h (10, 1)	[154]
Tp-Tg iCOF	Facilitate ion transport	1000 cycles, 99.69% (10, 1)	300 h (1, 10) DOD = 50%	[150]

deposition and promoting zinc dendrite growth. In contrast, following the introduction of rGO, the electrode conductivity is significantly enhanced by the rGO network, resulting in more uniform charge transport. This ensures a uniform electric field distribution surrounding the entire rGO network (Figure 5b). The uniform electric field distribution on the Zn/rGO@CC electrode effectively guides zinc ions to deposit uniformly on the rGO skeleton, thereby inhibiting the formation of zinc dendrites (Figure 5c).

In addition to rGO, nitrogen-doped graphene oxide (NGO) has also been used as AIL to protect Zn anodes. Hao et al. utilized NGOs as an artificial protective layer for the Zn anode to regulate the deposition of Zn²⁺ and the interfacial electric field distribution, thereby inhibiting the growth of dendritic crystals.^[92] Utilizing a one-step Langmuir–Blodgett technique, Zhou et al. successfully constructed an NGO protective layer on the zinc metal anode (Figure 5d).^[93] XPS analysis confirmed the presence of abundant pyridinic N (Npd), pyrrolic N (Npr), and

quaternary N (Nq) (Figure 5e), along with C=O and C-OH functional groups within the NGO layer (Figure 5f). These polar functional groups markedly increase the hydrophilicity of the NGO surface, leading to a marked enhancement in wettability at the NGO/electrolyte interface. This improved wettability promotes water molecule permeation, enhances Zn²⁺ diffusion and charge transfer kinetics, and consequently reduces polarization. Additionally, Yang et al. used a plasma-enhanced chemical vapor deposition strategy to achieve the direct growth of N/O co-doped carbon (NOC) AIL on the zinc anode.^[94] This conductive and ultrathin NOC coating combats dendrite growth via a dual mechanism. Primarily, it is responsible for the directed nucleation of Zn²⁺ at the interface, favoring zinc deposition on the energetically preferred (002) crystal plane. Concurrently, the rich heteroatoms within the NOC layer significantly lower the desolvation energy barrier for Zn²⁺ ions, thereby accelerating reaction kinetics. This synergistic action concurrently suppresses dendrite formation,

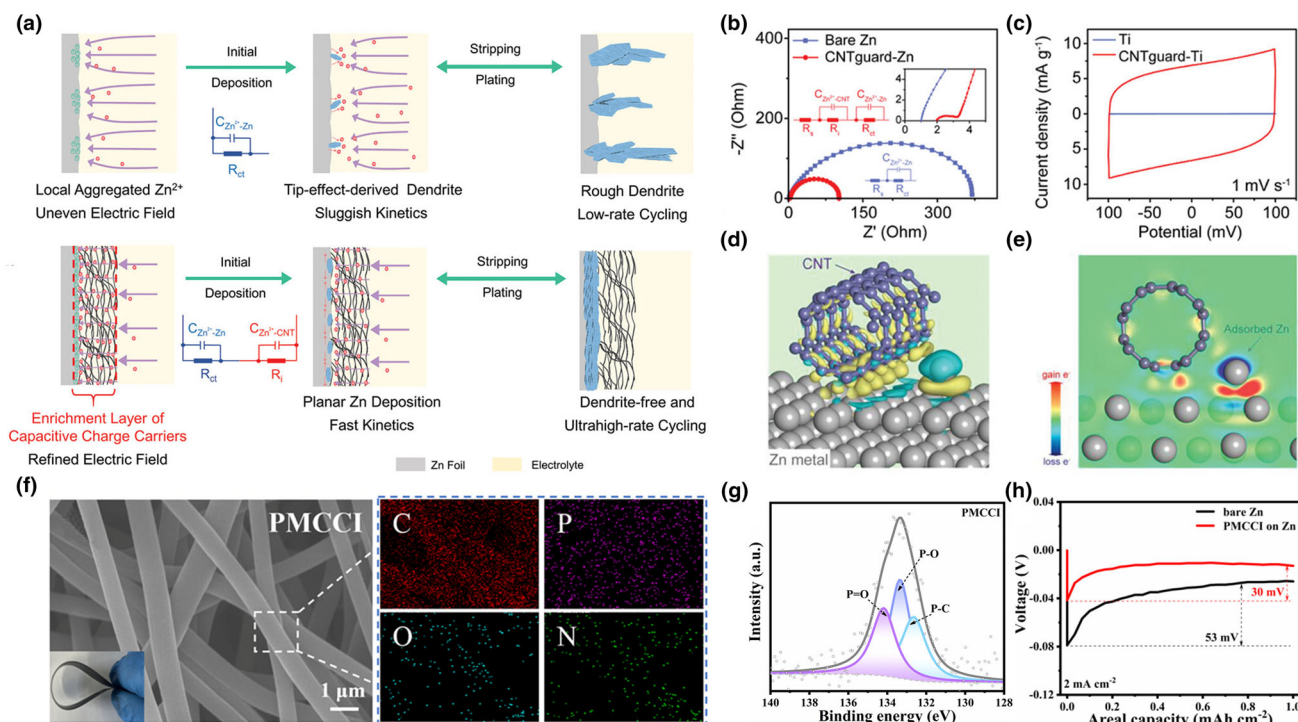


Figure 4. a) Schematic of bare Zn and optimized Zn during plating/stripping. b) The Nyquist plots and c) CV curves of optimized Zn. d) Charge density difference distribution and e) the corresponding sliced 2D contour map. Reprinted with permission.^[84] Copyright 2023, WILEY-VCH. f) SEM image and corresponding elemental mapping of PMCCI. g) The high-resolution P 2p XPS spectrum of PMCCI. h) Comparison of nucleation overpotentials of bare Zn and PMCCI@Zn. Reprinted with permission.^[86] Copyright 2024, WILEY-VCH.

HER, and corrosion. As a result, the assembled NOC@Zn symmetric cell demonstrates outstanding cycling stability, operating reliably at a high current density of 30 mA cm⁻² and 63% DOD, achieving ordered Zn²⁺ deposition on the anode even under demanding high-current conditions.

Graphdiyne (GDY) is a new 2D carbon material that combines sp and sp² hybridization.^[95] It has garnered significant interest in the area of AZMBs due to its distinctive electrochemical characteristics. GDY features a large π -conjugated structure that improves the charge transport speed during electrode reactions. Additionally, its uniform and porous structure, which includes a microscale cross-linking network, facilitates rapid diffusion of Zn²⁺. Huang et al. create an ultrathin vertically stacked GDY nanowall to develop a nanomesh interface on the surface of a zinc metal (Zn-VSGDY) electrode.^[96] The GDY nanowalls, which have interconnected structures, provide a semi-open nanostructure that is compatible with zinc. They serve as channels for ion conduction to facilitate the redistribution of Zn²⁺ flux, help mitigate the volume changes of the zinc anode, and promote the deposition of zinc within the nanowalls. This strategy integrates spatial ion control and a consistent deposition structure, effectively resulting in uniform and bottom-up zinc deposition. Another property of GDY is that it can be mildly and controllably grown on various substrates.^[95] This feature is beneficial for the precise fabrication and modification of high-performance interfaces, allowing for the preservation of the surface structure of the hosts. Liu et al. simultaneously applied GDY for the modification of both the anode and cathode in AZMBs.^[97] They engineered a novel all-graphdiyne-based zinc battery by synthesizing fluorinated GDY with trifluoro-substitution (3F-GDY). The porous 3F-GDY architecture enhances the Zn²⁺ diffusion at both electrodes, while the

interactions between F⁻ and Zn²⁺ facilitate the desolvation of hydrated Zn²⁺. This synergistically enhances the electrochemical reversibility and kinetics of the NVO cathode, concurrently inducing uniform zinc deposition on the anode. Li et al. utilized GDY's exceptionally high specific surface area as a heterojunction interface and introduced the innovative concept of GDY atomic electrodes. This strategy facilitates the orderly growth of metallic nanostructures by precisely controlling the nucleation sites. A pure zinc anode was used directly as the substrate for the in situ controlled growth of the GDY film through the cross-coupling reaction. During the initial stage of plating, three distinct peaks at 36.3°, 38.9°, and 43.2° were observed, corresponding to metallic zinc. The zinc atoms were selectively, uniformly, and stably anchored onto the GDY. As the deposition continues, the Zn atoms are encouraged to form larger clusters, which then develop into nanoplates, creating a new heterojunction interface on the GDY. This homogeneous nanoplate can be gradually dissolved during the stripping process, resulting in a progressive disappearance of the XRD peaks. This transition occurs as the material evolves from a nanoplate to Zn clusters and ultimately dissolves into individual atoms. A highly reversible and controllable process for zinc plating and deposition has been achieved.

In recent years, novel 2D transition metal carbides/nitrides (MXenes) have been identified as a promising candidate material for enhancing zinc anode performance.^[98] Obtained through the chemical etching of layered MAX phases, these materials have been identified as having great potential to improve zinc anode performance, due to their unique structures and properties. Niu et al. developed a simple in situ spontaneous reduction/assembly strategy to deposit a uniform MXene layer on the Zn anode surface.^[99] The MXene layer offers unique advantages, including a low nucleation barrier and a uniformly

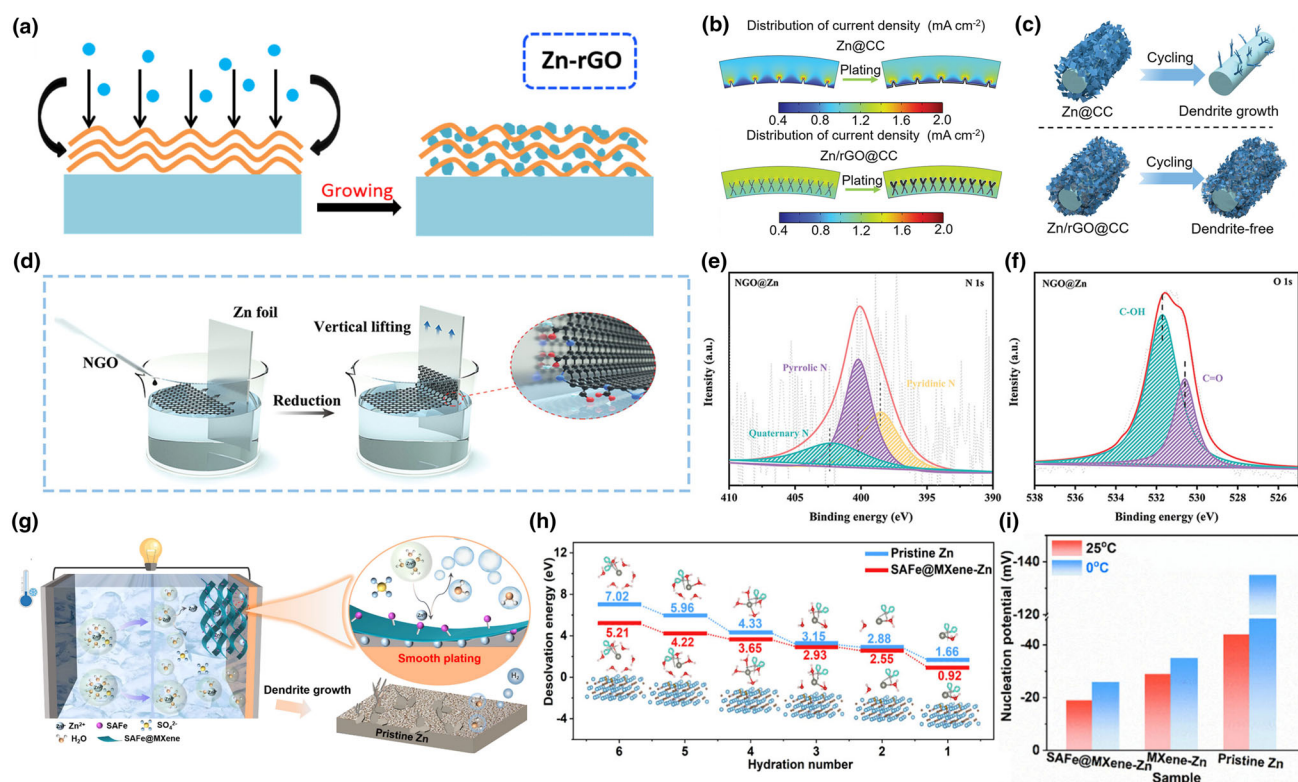


Figure 5. a) Illustration of the Zn plating behavior on the Zn-rGO anode. Reprinted with permission.^[90] Copyright 2019, Elsevier. b) Electric field simulation of Zn@CC with/without rGO. c) Zn plating/stripping behaviors under Zn@CC and Zn/rGO@CC. Reprinted with permission.^[91] Copyright 2023, WILEY-VCH. d) Schematic illustrations of fabricating ultrathin nitrogen-doped graphene oxide (NGO) on Zn metal foil. e) N 1s and f) O 1s XPS spectra of NGO@Zn. Reprinted with permission.^[93] Copyright 2021, WILEY-VCH. g) Schematic illustration of SAFe@MXene to promote smooth Zn plating. h) Comparison of [Zn(H₂O)₆]²⁺ desolvation barriers with/without SAFe@MXene. i) Comparison of Zn nucleation on the SAFe@MXene-Zn, MXene-Zn, and pristine Zn electrodes. Reprinted with permission.^[100] Copyright 2025, American Chemical Society.

distributed electric field, which facilitates homogeneous zinc deposition. As a result, the MXene-modified Zn anode demonstrates long-term cycling stability, diminished voltage hysteresis, and a smooth, dendrite-free surface. Furthermore, as a 2D material analogous to graphene, MXenes possess defect-rich interfaces that accommodate additional single metal atoms. This incorporation induces orbital hybridization and increases interfacial distortion, thereby enhancing the number of active sites. Accordingly, Wang et al. employed highly active single-atom catalysts on MXene to construct an AIL, which promotes Zn²⁺ desolvation and diffusion (Figure 5g), thereby counteracting dendritic growth.^[100] The defect-rich Ti₃C₂T_x nanosheets, anchoring iron atoms (designated as SAFe@MXene), form a catalytically modulated layer that exerts a pronounced catalytic effect. Density functional theory (DFT) calculations revealed that [Zn(H₂O)₆]²⁺ at the SAFe@MXene-Zn/electrolyte interface required merely 5.21 eV to completely release the water solvent, while as high as 7.02 eV was necessary for the pristine Zn/electrolyte interface (Figure 5h). The assembled atom-on-MXene weakens the interaction of Zn²⁺-H₂O bonds, facilitating fast desolvation and simultaneously inhibiting HER occurrence and dendrite growth. Consequently, the SAFe@MXene-Zn anode accelerates Zn²⁺ nucleation kinetics, achieving an impressively low overpotential of 19 mV (Figure 5i).

Graphitic carbon nitride (g-C₃N₄) is an emerging synthetic 2D carbon material with its unique nanopore structures and abundant

nitrogen sites.^[101] These features allow it to effectively bind metal ions (e.g., Li⁺, Na⁺, and Zn²⁺) and have attracted significant attention in the field of energy storage.^[102,103] Zhang et al. employed g-C₃N₄ as a multifunctional protective coating to stabilize zinc metal anodes.^[104] The nitrogen-rich g-C₃N₄ exhibits intrinsic zincophilic properties, whereby Zn²⁺ bonds with N atoms to form Zn-N coordination, thereby inducing uniform nucleation of metallic zinc. Additionally, g-C₃N₄ exhibits strong Lewis basicity. The incorporation of the P element enhances the Lewis basicity of the g-C₃N₄ framework while simultaneously weakening the interactions between Zn²⁺ and H₂O. Wang et al. constructed a layer of phosphorus-doped g-C₃N₄ (PCN) on the zinc metal surface, which has been shown to significantly enhance the reaction kinetics and cycling stability of zinc anodes.^[103] Additional analysis of PCN particles shows that zinc atoms become integrated into the structure, resulting in the formation of Zn-intercalated PCN (ZPCN) complexes. The ZPCN complex significantly lowers the energy barrier for zinc diffusion, facilitating uniform plating and stripping while effectively preventing the growth of zinc dendrites.

The regulated growth of 2D carbon materials on substrates allows for the creation of effective interfaces and their adjustable chemical structure, combined with a distinctive electron and ion transport network, which facilitates precise control of reactions at the atomic level. The use of 2D carbon materials in AZMBs is limited due to the complicated and expensive manufacturing process. In the future, developing

graphene-based zinc anode interphases will be crucial for achieving significant improvements in the reversibility of zinc metal electrodes. Moreover, the advancement of 2D carbon material engineering at the zinc anode interface will also play a crucial role in enhancing the performance of AZMBs.

3.1.3. 3D Carbon Materials

The porous architecture of commercially available 3D carbon materials is commonly used as a structural scaffold for zinc deposition. The 3D interconnection framework of loosely stacked graphite nanosheets exhibits epitaxial deposition control properties similar to those of graphene. Hou et al. developed a highly stable Cu-Ps/EG composite matrix by embedding zincophilic copper nanoparticles, which were dispersed uniformly, within an expanded graphite (EG) framework (Figure 6a).^[105] In this particular Cu-Ps/EG system, the nano-scale Cu particles are distributed uniformly on and between the layers of graphite, acting as zincophilic seeds for reducing the Zn nucleation overpotential (Figure 6b). The configuration provides adequate space for zinc deposition, thereby reducing the risk of the framework collapsing due to alterations in volume that may occur during repetitive plating/stripping processes (Figure 6c). Zhi et al. innovated the design of CF substrates with gradient-distributed Cu nanoparticles (CF-G-Cu NPs) (Figure 6d).^[106] The contact angle of the modified electrode was significantly reduced from 122° (original CF) to 99.6° (Figure 6e) due to the enhanced capillary effect of the loaded nanoparticles in the CF substrate. The gradient distribution of Cu ensured a more homogeneous electric field, thereby directing the Zn^{2+} flux more uniformly

throughout the collector, favoring deeper and more controlled zinc deposition. Potential and current density distributions of pristine CF and CF-G-Cu NPs are shown by finite element method simulations (Figure 6f). The pristine CF surface showed the highest electric field concentration (8.42 V m^{-1}) and current distribution (2.1 mA cm^{-2}). In contrast, the modified current collector showed a significant electric field gradient (8.42–0.474 V m^{-1}) and current distribution (2.1–0.119 mA cm^{-2}) (Figure 6g). This gradient distribution is crucial for the uniform distribution of Zn^{2+} . It facilitates the achievement of uniform Zn coating throughout the internal structure of the carbon mats, not only at the bottom of the mats. Regarding side reaction inhibition, constructing hydrophobic micro-regions can enhance Zn^{2+} conduction while effectively preventing side reactions at the electrode/electrolyte interface. Meng et al. prepared an ultrathin zinc-carbon composite anode by co-coiling cellulose-exfoliated graphene (CEG) with zinc foil.^[107] This 3D interpenetrating structure can generate hydrophobic microdomains at multiple solid-liquid interfaces. A laser Raman spectrometer was used to detect the distribution of by-products (Figure 6h). Following a 24 h immersion of the Zn foil in the electrolyte at the same intensity scale, the signal intensity was found to be vigorous in the majority of regions. This finding indicates that a significant quantity of $\text{Zn}_4\text{SO}_4(\text{OH})_6 \cdot 5\text{H}_2\text{O}$ (ZHS) was distributed unevenly across the surface. However, the signal intensity on the Zn@CEG surface remained extremely weak across the entire observed range, indicating that the introduction of CEG hindered the corrosion reaction from occurring.

The issue of dendrite growth at the anode interface represents a significant challenge in the construction of both safety and high-longevity AZMBs. Carbon materials have unique advantages in regulating the

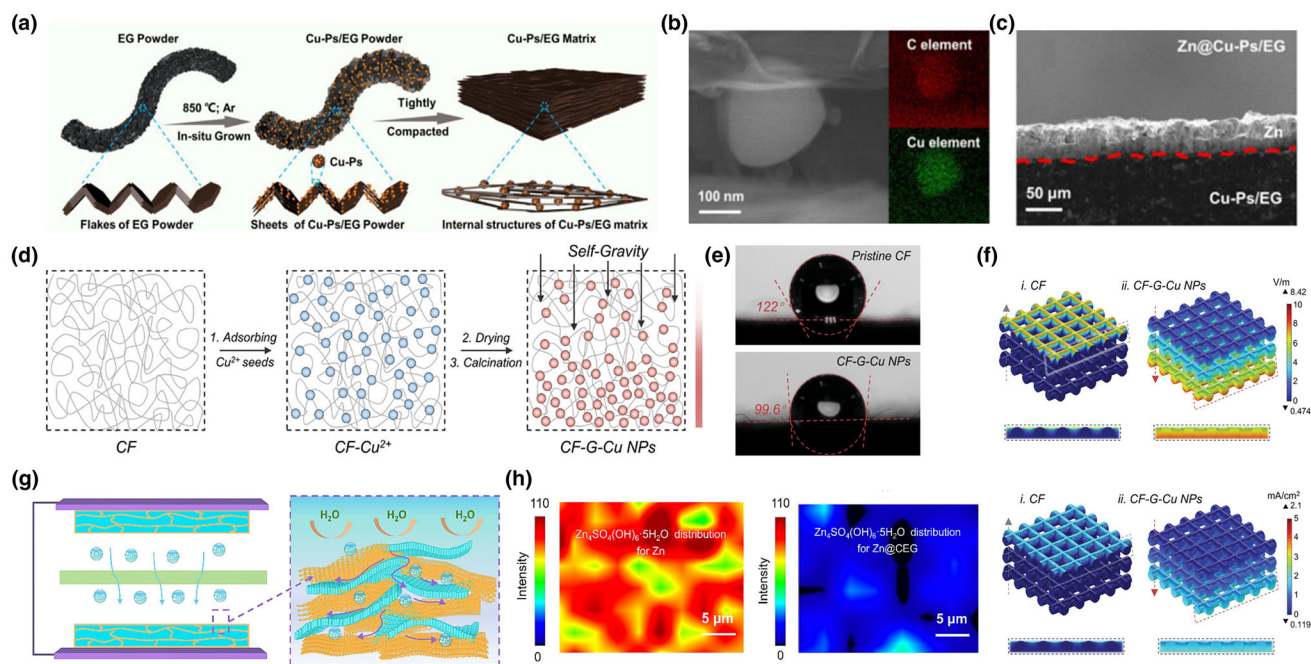


Figure 6. a) Schematic illustration of the synthesis of Cu-Ps/EG matrix. b, c) Cross-section SEM and corresponding elemental mappings of Cu-Ps/EG matrix. Reprinted with permission.^[105] Copyright 2022, Elsevier. d) Schematic of the formation process of CF-G-Cu NPs. e) Contact angle results of CF and CF-G-Cu NPs. f) Simulations of the zinc plating on pristine CF and CF-G-Cu NPs substrates. Reprinted with permission.^[106] Copyright 2024, WILEY-VCH. g) Illustration of the corrosion protection mechanism of electrodes in the Zn@CEG-based cell. h) Colorful image of Zn and Zn@CEG after 24 h immersion in 2 M ZnSO_4 electrolyte. Reprinted with permission.^[107] Copyright 2023, Elsevier.

interfacial electric field distribution and homogenizing the zinc-ion flux due to their excellent electrical conductivity. Concurrently, their mechanical structure can also inhibit dendrite growth. However, the overly superior electrical conductivity of conventional carbon materials can be detrimental to zinc-ion deposition. The Zn^{2+} tends to deposit on the coating surface rather than on the zinc metal surface, which leads to dendrite growth and HER on the Zn anode surface. Future research should focus on modulating the structure of carbon materials to improve zinc deposition behavior within the coating, which is essential for achieving uniform zinc deposition.

3.2. Zincophilic Alloys

Electrochemical processes occur at the interface between the zinc anode and the electrolyte and are influenced by the microstructure of the anode surface.^[108] Most studies have assessed deposition performance by the final morphology of the anode but have often neglected the initial nucleation and growth processes. Zincophilic alloys offer excellent potential for improving the performance of AZMBs. The addition of selected alloying elements into the zinc substrate enables precise modulation of the nucleation and growth behaviors of zinc atoms.^[109] Current zinc anode alloying strategy includes two main approaches: 1) introducing high-affinity alloying elements to the zinc metal surface to increase active nucleation sites, thereby promoting uniform zinc deposition and 2) direct modification of the zinc matrix to induce precipitation of dispersed alloying phases, which can inhibit the intergranular corrosion while refining the grains.^[110]

3.2.1. Zincophilic Alloys for Surface Modification

Introducing dispersed metal particles as nucleation sites can effectively reduce the nucleation energy barrier of Zn^{2+} , thus improving the Zn deposition behavior. Cui et al. used ion beam sputtering to deposit Au nanoparticles on the Zn surface (Figure 7a).^[111] By regulating the electric field distribution, Zn^{2+} was guided to nucleate uniformly, forming sheet-like Zn arrays and effectively suppressing irregular protrusions (Figure 7b). However, due to weak interfacial adhesion, physical sputtering coatings are prone to delamination over extended periods. To overcome this limitation, Daria et al. used an in situ substitution method to prepare Ag-Zn₃ alloy layers (Figure 7c).^[112] The Ag-Zn₃ alloy phase exhibits excellent Zn affinity, which reduces the nucleation barrier and improves the cycling stability (Figure 7d). However, it should be noted that the effectiveness of a single metal protective layer is limited. The introduction of a dense, heterogeneous metal protective layer can hinder the diffusion of Zn^{2+} on the electrode surface and increase the charge transfer impedance. The combined effect of multiple alloy anodes has been shown to comprehensively enhance anode performance. Liu et al. proposed an in situ evolutionary metal alloy interfacial phase strategy to form Zn@Ag-In that can protect metal zinc anodes in real time (Figure 7e).^[113] Distinct electrode processes during zincophilic alloying were analyzed using distribution of relaxation times (DRT) analysis of EIS, revealing their polarization contributions (Figure 7f). As the alloying process proceeds, the mobility of zinc ions within the metal interface layer increases. A vital phenomenon observed from the DRT plots is the emergence of a weak peak at approximately 10^{-4} s, which indicates the gradual formation of the metal interalloy phase at the surface of the Zn@Ag-In electrodes. After 10 cycles, a more

pronounced peak at the exact location is observed, implying a stable alloy phase formation within the alloy layer (Figure 7g). This Ag_xZn_y-In alloy phase has an SEI similar to that in LIBs, which promotes uniform and directional deposition on the surface of Zn(002) crystals and accelerates Zn^{2+} migration, thereby regulating the Zn^{2+} plating process.

Jiang et al. designed lamellar Zn/Al₂O₃ core-shell nanostructures based on the eutectic compatibility of Zn-Al (Figure 7h).^[114] The more active aluminum metal in situ forms an Al₂O₃ protective layer during the battery cycling process, which in turn effectively promotes the uniform deposition of metallic zinc and reduces the formation of inert by-products, such as ZnO or Zn(OH)₂. In addition, the insulating Al₂O₃ protective layer effectively prevents zinc from being deposited on the surface. The result is that the zinc can be uniformly deposited in the designed pits. In terms of corrosion inhibition, Pb metal has a good effect. The Pb-based interface (containing Pb/Pb(OH)₂/PbSO₄) is constructed through a substitution reaction (Figure 7i), and its low HER activity and high H⁺ tolerance can block the corrosion of H⁺ on Zn substrates.^[115] Importantly, the Pb(OAc)₂ additive precipitates with SO₄²⁻ to PbSO₄ and releases trace amounts of Pb²⁺ to activate Pb plating/stripping to build Pb-containing layers on the Zn plating, thus consistently inhibiting HER throughout the cycle and improving the reversibility of AZMBs (Figure 7j).

3.2.2. Zincophilic Alloys for Bulk Phase Engineering

In recent years, although surface modification of zinc by introducing metal particles has been widely reported, direct alloying modification of the zinc bulk phase is becoming a more effective strategy. The electrochemical properties of zinc anodes are mainly governed by three key factors: chemical composition, phase composition, and microstructure. Alloying the zinc matrix with selected elements can reconfigure the zinc matrix microstructure and precisely regulate the physicochemical properties of the zinc metal. Examples include re-exposure of specific crystal planes, grain refinement, and modulation of phase composition at the grain boundaries (GBs). Taking zinc-bismuth alloys as an example, He et al. successfully synthesized zinc-bismuth (Zn-Bi) alloys with a specific crystal orientation that preferentially exposed the (002) crystal surfaces using melt processing.^[116] This structural feature has two advantages: on the one hand, more (002) crystal surfaces are favorable for the epitaxial deposition of Zn^{2+} ; on the other hand, the alloying treatment refines the grain structure and improves the interfacial electric field distribution. This synergistic effect not only inhibits the growth of Zn dendrites but also optimizes the deposition behavior, significantly improving the cycling stability of the electrode.

GBs, as highly active regions, serve as both preferential diffusion channels for Zn^{2+} and provide heterogeneous nucleation conditions for Zn deposition (Figure 8a). However, in weakly acidic aqueous electrolytes, zincophilic alloys encounter significant self-corrosion issues, primarily attributed to the segregation and precipitation of alloying elements at GBs. According to the thermodynamics of corrosion, the free energy generated by grain refinement reduces the cell potential, making the material more susceptible to electrochemical dissolution in a given corrosive environment.^[117] In other words, ultrafine-grain structures with high-density GBs are more susceptible to corrosion than coarse-grain structures. Therefore, grain refinement should strike a balance between the number and stability of GBs. While ensuring a sufficient density of GBs to facilitate ionic transport, it is equally imperative to account for the risk of intergranular corrosion that may arise from

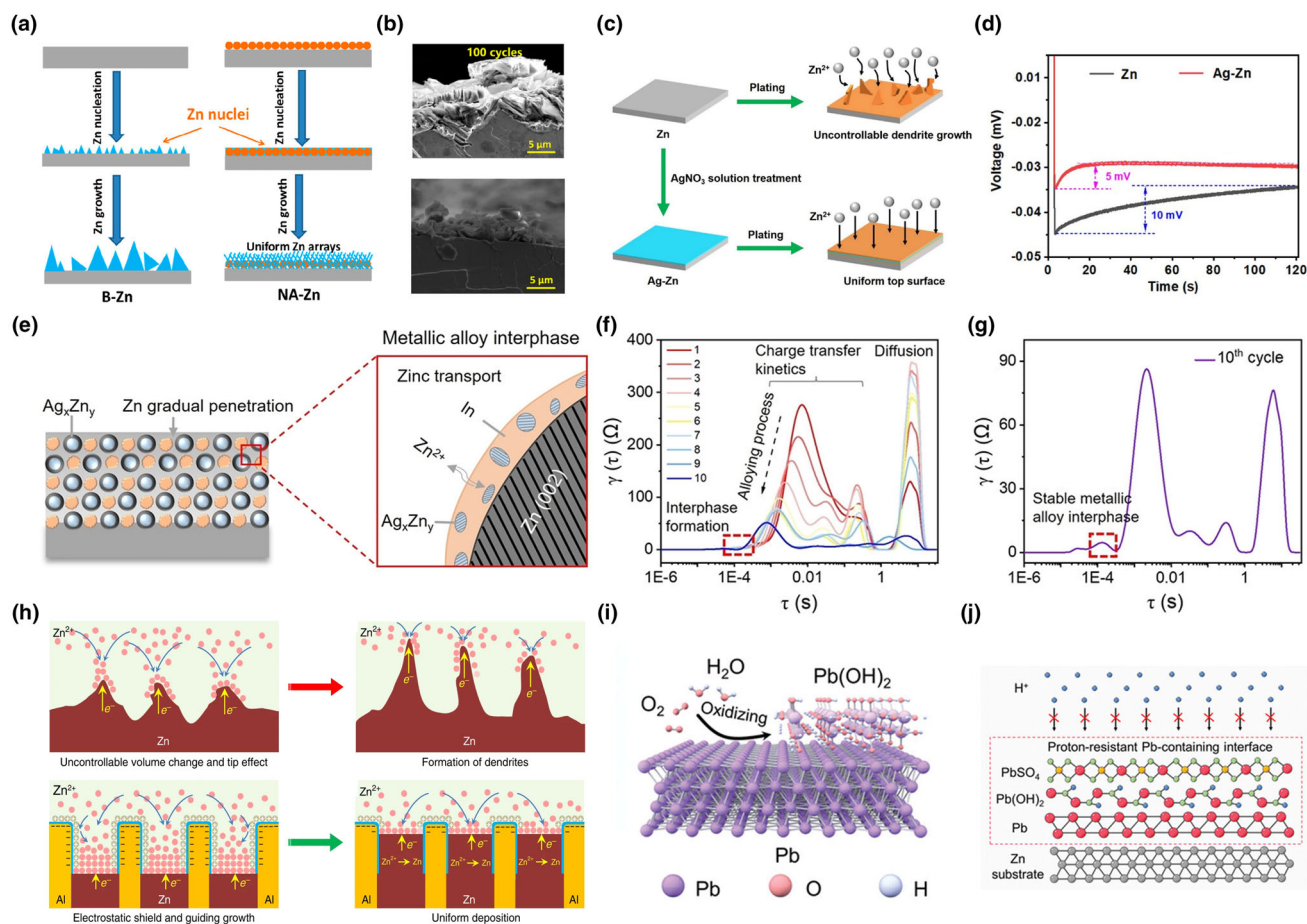


Figure 7. a) Schematic illustration of the Zn plating/stripping of NA-Zn and corresponding b) SEM images. Reprinted with permission.^[111] Copyright 2019, American Chemical Society. c) Schematic illustration of Ag-Zn on Zn plating. d) Zn nucleation on untreated Zn and Ag-Zn. Reprinted with permission.^[112] Copyright 2021, American Chemical Society. e) Schematic diagram of the evolution of the dual-heterometallic interlayer during zinc plating/stripping processes. f) The corresponding DRT plots of the Zn@Ag – In/Zn@Ag – In. g) The DRT plot after 10 cycles. Reprinted with permission.^[113] Copyright 2024, Wiley-VCH. h) Schematic of monometallic zinc electrodes and eutectic Zn/Al alloy electrodes. Reprinted with permission.^[114] Copyright 2020, Springer Nature. i) Schematic illustration of the preparation process of Zn@Pb and j) proton-resistant Pb-containing interface. Reprinted with permission.^[115] Copyright 2023, WILEY-VCH.

an excessive proliferation of such boundaries. In response to this key problematic issue, researchers have proposed an innovative strategy to inhibit zinc self-corrosion by modifying the chemical properties of GBs. Zhou et al. successfully designed a Zn-Ti biphasic alloy system.^[110] The introduction of TiZn₁₆ intermetallic compounds, which can stabilize GBs, can inhibit grain boundary corrosion and regulate Zn²⁺ deposition kinetics. Comparing and analyzing the electron backscatter diffraction inverse pole figure (EBSD IPF) imaging results of bare Zn and Zn-Ti alloys in the pristine state and after immersion for 24 h (Figure 8b), significant differences in the corrosion behaviors can be observed. The phase identification of the Zn-Ti alloy decreased slightly, from 98% to 95%, after immersion, indicating excellent phase stability. In comparison, the recognizable phase of bare Zn decreased from close to 100% to 89%, indicating that its structure was severely damaged during immersion (Figure 8c). This significant difference in performance is primarily attributed to the stable presence of TiZn₁₆ intermetallic compounds at the GBs of Zn-Ti alloys, which optimizes the local electronic structure to block the corrosion expansion path along the GBs. In terms of regulating the deposition kinetics, this

thermodynamically stable TiZn₁₆ alloy phase at GBs achieves the gradual activation of the nucleation sites by reducing the Gibbs free energy of the nucleation phase and matching it with the growth phase, which contributes to the formation of a flat and homogeneous microstructure of the zinc deposition layer (Figure 8d). Chen et al. utilized the rare earth element cerium (Ce) to construct an ultrafine rare earth alloy layer (URAL) on the surface of a Zn foil (Figure 8e).^[118] The addition of Ce can refine the grains and increase the number of nucleation sites. Moreover, Ce can also stabilize the zinc anode GBs by using the “pinning effect.” First-principles calculations were employed to evaluate the reactivity of zinc atoms within the grains and at the GBs. The similarity in reactivity between the Zn (10 $\bar{1}$ 1) and Zn (0002) crystal planes, while the Esite at the GBs is significantly higher than that within the crystal. This observation suggests that the Zn-electrolyte reaction is more favorable at the GBs, indicating that the Zn²⁺ tends to diffuse along the GBs (Figure 8f). When Ce atoms are introduced into GBs, they tend to separate at GBs due to their larger atomic radii. At the interface between the CeZn₃ (20 $\bar{2}$ 0) and Zn (0002) planes, the Esite of Zn atoms rises from 1.35 to 1.85 eV, which indicates an increase in the energy barrier for

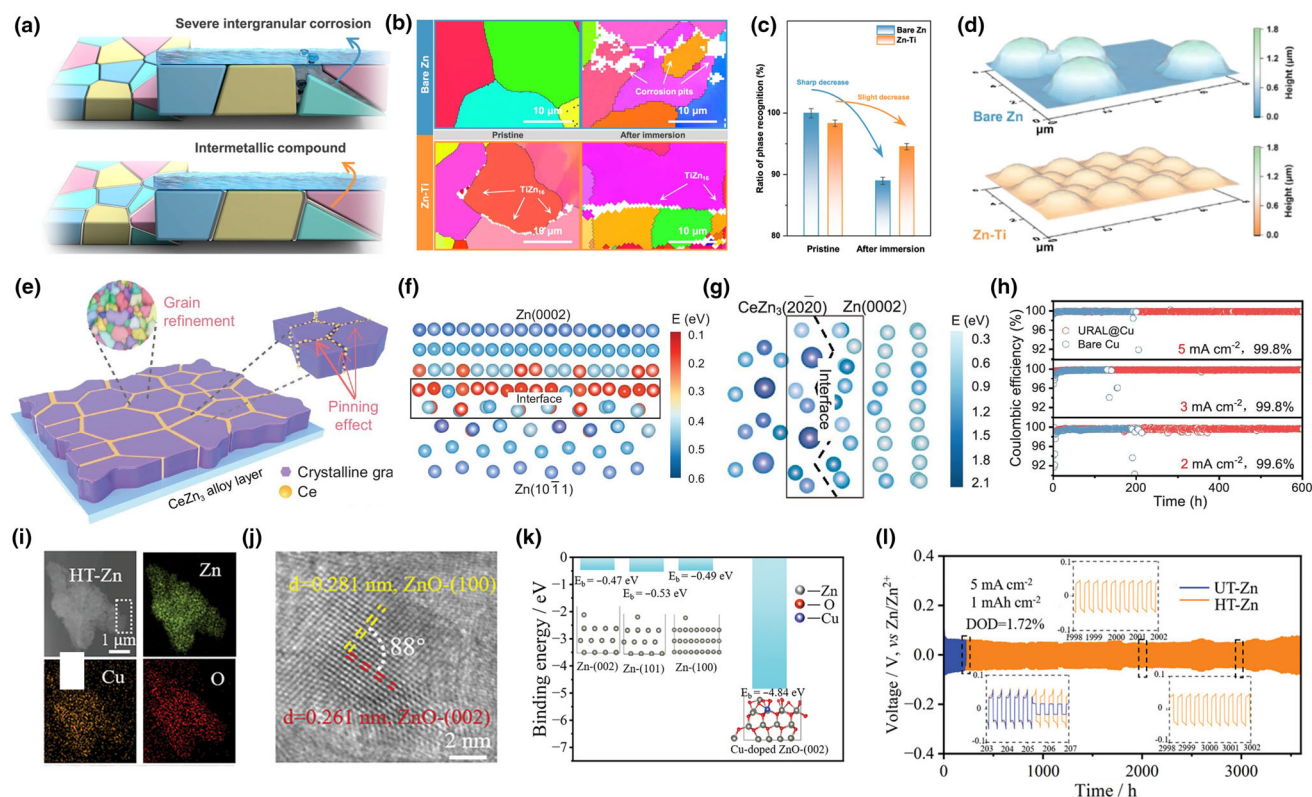


Figure 8. a) Schematic illustration of GBE. b) EBSD IPF mapping images of Zn anodes after 24 h of immersion. c) Corresponding ratio of phase recognition based on image identification. d) Zn deposition models after 240 s of plating. Reprinted with permission.^[110] Copyright 2023, Springer Nature. e) Schematic illustration of the preparation mechanism for URAL. f) Esite of Zn atoms in Zn(0002), Zn(10 $\bar{1}$ 1), and their interface. g) Esite of Zn atoms in CeZn₃(20 $\bar{2}$ 0), Zn(0002). h) CEs for URAL@Cu electrodes and bare Cu electrodes. Reprinted with permission.^[118] Copyright 2024, Oxford University Press. i) STEM-EDS elemental mapping of HT-Zn. j) HRTEM lattice imaging. k) Binding energies of Zn atoms on different crystal faces and Cu-doped ZnO (002) faces. l) Voltage profiles of HT-Zn and UT-Zn at 5 mA cm⁻². Reprinted with permission.^[119] Copyright 2025, WILEY-VCH.

the Zn reaction. The bias of the rare earth elements at the GBs increases the potential energy of the GBs (Figure 8g), which inhibits the corrosion. Consequently, the assembled ZnCellCu asymmetric cell exhibits an excellent CE (Figure 8h).

Recent findings suggest that introducing exogenous surface materials can impact the durability of the interface due to structural heterogeneity, thereby disrupting long-term plating/stripping. To break through this limitation, Yuan et al. devised a novel self-activation method for controllable zinc plating using the Cu impurities inherent in commercial zinc foils to generate Cu-rich surfaces as nucleation sites.^[119] Mild heat treatment of naturally oxidized zinc foils mobilizes subsurface Cu atoms and migrates them to the surface under the influence of ambient oxygen conditions. Scanning transmission electron microscopy-energy dispersive X-ray spectroscopy (STEM-EDS) and high-resolution transmission electron microscopy (HRTEM) confirm the Cu enrichment of the zinc surface (Figure 8i,j), while DFT calculations demonstrate the high affinity of this Cu-rich layer for zinc (Figure 8k). This affinity layer reduces the nucleation barrier and enhances the transport kinetics of Zn²⁺ during deposition. In situ 3D microscopy reveals that the Cu-rich surface promotes dense Zn growth without dendrites and with (101) orientation. As a result, the Zn||Zn symmetric cells constructed in this way can be operated stably for more than 3600 h at 5 mA cm⁻² and 1 mAh cm⁻², exhibiting an excellent cycling durability (Figure 8l).

Zincophilic alloys offer several advantages, including compositional diversity and the ability to control the addition of alloying elements. This enables comprehensive regulation of dendrite growth, HER, and corrosion from multiple perspectives. Current research has expanded from binary zincophilic alloy systems to multi-component alloy systems, and in the future, more alloying elements can be introduced. Even the high-entropy alloys can be designed, which can further coordinate multiple elements.^[108] This alloying element design strategy is expected to significantly enhance the cycling stability of zinc anodes and offer new insights for the development of next-generation high-performance AZMBs.

Although carbon materials and zincophilic alloys can modulate the interfacial electric field distribution and provide nucleation sites for the homogeneous deposition of Zn²⁺, they both suffer from a problem. Zinc deposition is directly exposed to the electrolyte. It is not effectively insulated from the possibility of reactive water molecules contacting the electrons, making it difficult to suppress dendrite growth and HER. An alternative and effective strategy to address this issue involves constructing an ion-conductive but electronically insulating AIL on the surface of the zinc anode, thereby reducing the contact area between the electrode and the electrolyte to inhibit side reactions. In addition, the use of AIL materials with a porous structure not only restricts the disordered diffusion of carriers but also optimizes the zinc-ion flux distribution and promotes the uniform deposition of zinc. According to the material

system, they are categorized into two main groups: inorganic compounds and organic compounds.

3.3. Inorganic Compounds

Inorganic compounds present at the interface of the zinc anode primarily function as “electron shielding” through the porous structure. This enables precise regulation of the migration path of carriers and isolation of direct contact between active water and the electrode. Some inorganic compound materials can also form a local electric field via spontaneous polarization effect, which significantly enhances the transport kinetics of zinc ions. Based on the difference in chemical composition, inorganic compounds are classified into oxide and non-oxide systems.

3.3.1. Inorganic Oxides

As zinc anode interface modification materials, inorganic oxides effectively regulate the Zn^{2+} deposition behavior and inhibit the side reactions by constructing physical barriers and ion transport channels. As representatives, porous materials such as kaolin^[120] and CaCO_3 ^[121] can act as physical barriers to separate the aqueous electrolyte from the zinc anode. Furthermore, the uniform distribution of pore size has been shown to homogenize the Zn^{2+} flux. Zhi et al. reported a cost-effective, simple, and porous CaCO_3 coating, which can be used as a buffer layer (Figure 9a).^[121] The porous structure of the CaCO_3 ensures that the plating process is confined to the coated area of the zinc anode, thereby ensuring a consistent plating rate across the entire zinc metal surface. This process ensures a uniform, bottom-up galvanizing process, thereby avoiding the development of dendritic growth, which can lead to large polarization and battery short circuits. However, due to the steric hindrance effect, the limited pore size severely impedes the rapid transport of Zn^{2+} , making Zn^{2+} migration within the nanopores still challenging under extreme conditions such as high current densities and large deposition capacities. Furthermore, the high desolvation energy barrier has a detrimental effect on the efficiency of ion transport, resulting in a marginal improvement in Zn^{2+} transport kinetics.

To ensure the rapid diffusion of zinc and promote uniform zinc deposition, the ion transport kinetics within the interfacial layer should be optimized. Inspired by the Maxwell-Wagner polarization effect, the polarization induced by the separation of space charges between two media with different dielectric constants and conductivities can generate a local electric field that accelerates the transport of carriers. For instance, ZrO_2 coatings with high dielectric constants facilitate uniform and dense zinc deposition (Figure 9b).^[122] On the one hand, the ZrO_2 coating promotes the diffusive transport of Zn^{2+} through the Maxwell polarization effect and provides a stable and controlled nucleation environment. On the other hand, the uniform distribution of ZrO_2 nanoparticles on the Zn anode reduces the direct contact between the electrolyte and the metal surface and inhibits the occurrence of HER. Consequently, the ZrO_2/Zn electrode exhibits a smooth and uniform surface after cycling (Figure 9c). Similarly, Hur et al. created an artificial Nb_2O_5 layer on the zinc surface to promote uniform Zn deposition behavior (Figure 9d).^[123] Nb_2O_5 with a high dielectric constant can produce a strong dielectric polarization under the influence of an electric field. The adsorption of Zn^{2+} on the Nb_2O_5 layer involves a relatively low energy barrier (Figure 9e), which facilitates rapid and uniform electron transfer and Zn deposition.

Ferroelectric materials represented by BaTiO_3 ^[124] and β -phase poly(vinylidene fluoride)^[125] have been used as AILs to regulate the Zn deposition behavior. The ferroelectric electrodes are polarized with switchable spontaneous polarization domains, which can be oriented and aligned to form a localized strong electric field under an applied voltage. This localized strong electric field can enhance the Zn^{2+} transport kinetics and promote its rapid directional diffusion, leading to uniform and lateral deposition.^[126] Zhang et al. achieved the horizontal growth of Zn through a BaTiO_3 coating with ferroelectric properties (Figure 9f).^[124] The polarized BaTiO_3 coatings facilitated uniform channels for Zn^{2+} migration to the metal Zn surface, thereby improving the anodic transport kinetics. In addition, Chen et al. utilized tetragonal $\text{KTa}_{0.54}\text{Nb}_{0.46}\text{O}_3$ (t-KTN) to control the growth of zinc.^[127] In ferroelectric tetragonal KTN crystals, Nb^{5+} exhibits an eccentric displacement along the crystallographic direction, thereby inducing spontaneous polarization (Figure 9g). During the plating process, the negatively charged ferroelectric surface, oriented opposite to the polarization direction, attracts high concentrations of Zn^{2+} , thereby promoting dense and uniform deposition at the electrochemical interface. The confocal laser scanning microscope (CLSM) reveals that the surface height difference of the t-KTN layer is only 16.18 μm (Figure 9h,i), indicating that the t-KTN layer can effectively regulate the diffusion of Zn^{2+} and inhibit the growth of dendritic grains at the electrode interface.

While dendritic zinc growth is widely recognized as impairing the stability of zinc metal anodes, side reactions can also reduce the lifespan and performance of AZMBs. In aqueous electrolytes, Zn^{2+} typically exists in the form of a hexahydrated complex, $[\text{Zn}(\text{H}_2\text{O})_6]^{2+}$, whose structure is stabilized by coordination bonds with water molecules.^[128] The desolvation process involves breaking these coordination bonds to produce “bare” Zn^{2+} , a process analogous to a chemical reaction. To promote the desolvation of Zn^{2+} and inhibit the side reactions, researchers have investigated materials that can adjust the interfacial electric field and ion transport kinetics. Pan et al. reported that inorganic ferroelectric barium titanate (IF-BTO) coatings with aligned dipole-induced electric fields can facilitate Zn^{2+} desolvation (Figure 10a).^[129] Raman spectroscopic analysis across various depths and lateral positions within the IF-BTO layer confirms its role in facilitating the desolvation and aggregation of $[\text{Zn}(\text{H}_2\text{O})_6]^{2+}$ complexes (Figure 10b). In the presence of a polarized electric field, zinc ions exhibited a vertical migration trajectory while the zinc-ion solvation structure underwent an aggregation process before approaching the surface of the Zn metal (Figure 10c). The electric field induced by aligned dipoles can promote Zn^{2+} desolvation, modulate the transport behavior of Zn^{2+} , and remarkably eliminate water-related side reactions and Zn dendrites. Similarly, Yang et al. designed a zinc niobate (ZNB) dielectric ion-conducting layer to accelerate interfacial desolvation and regulate deposition kinetics (Figure 10d).^[130] In situ sum-frequency generation (SFG) spectroscopy showed that the solvent-water bonding at the ZNB/Zn interface was weakened, suggesting that the desolvation was facilitated (Figure 10e). The ZNB coating increased the Zn^{2+} transfer number from 0.170 to 0.549 (Figure 10f), which was attributed to its uniform pore size of 2–3 nm, allowing for the lateral diffusion of Zn^{2+} . As a result, the overpotential of the ZNB/Zn symmetric cell was reduced by 55.9%, and the cell could be recycled for 2000 h at 1 mA cm^{-2} . Layered zinc silicate (LZS) nanosheets with zincophilic sites and nanochannels were developed as an artificial SEI (Figure 10g) by Cheng et al.^[131] Theoretical and experimental analyses demonstrated that the LZS could reorganize the solvation shells of $[\text{Zn}(\text{H}_2\text{O})_6]^{2+}$, reduce the barrier to dissolution, and enhance the Zn^{2+} transport.

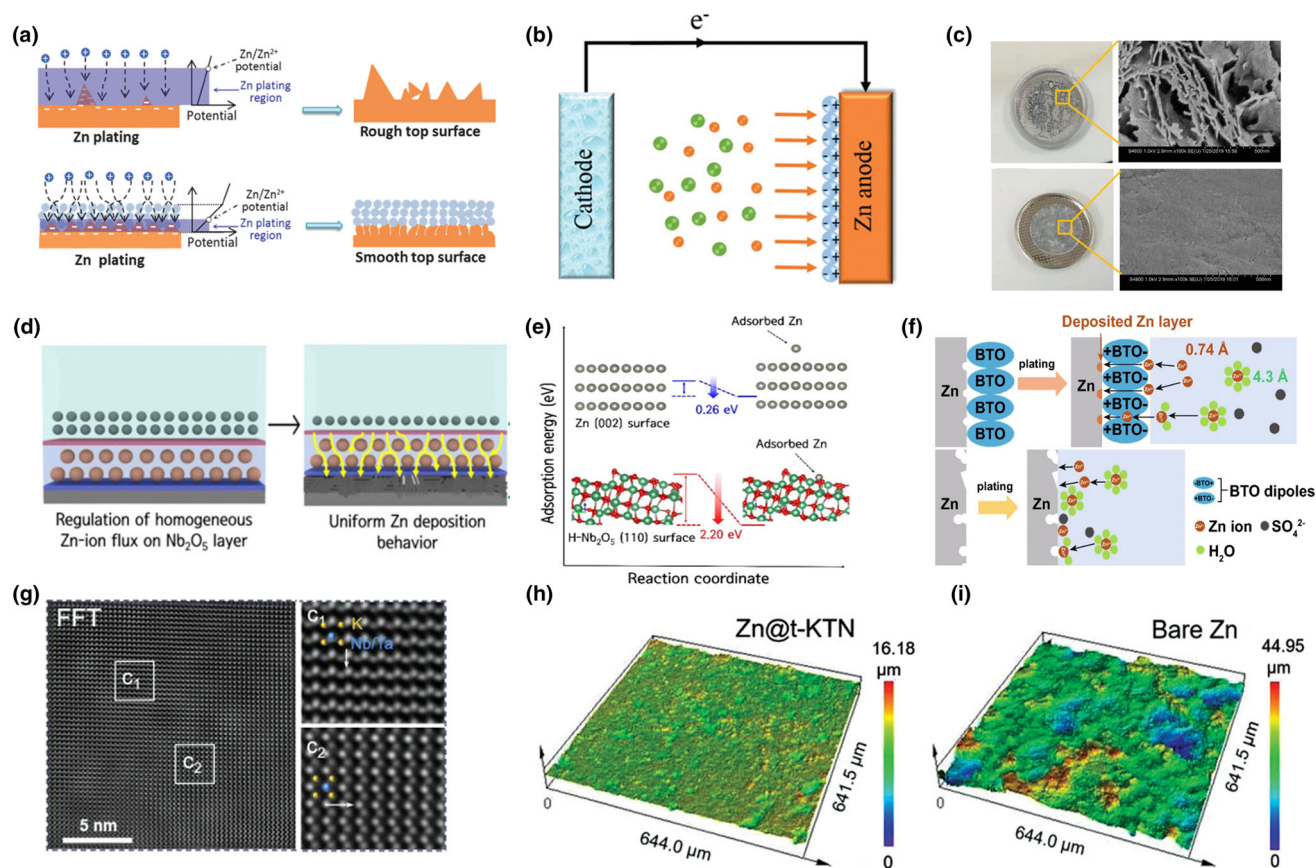


Figure 9. a) Schematic illustration of the Zn plating/stripping with nano- CaCO_3 coating. Reprinted with permission.^[121] Copyright 2018, WILEY-VCH. b) Schematic illustration of the Zn plating/stripping with ZrO_2 coating. c) Digital and corresponding SEM images. Reprinted with permission.^[122] Copyright 2019, WILEY-VCH. d) Schematic representation of uniform and directional deposition of Zn from Nb_2O_5 layer. e) Changes in energy level for Zn adsorption on Zn (002) and H- Nb_2O_5 (110) layers.^[123] Copyright 2022, Elsevier. f) Schematic representation of the transport mechanism of zinc ions at the BTO@Zn/electrolyte interface. Reprinted with permission.^[124] Copyright 2021, Springer Nature. g) Fourier transformed electron diffraction pattern of t-KTN. h, i) CLSM images of cyclic Zn@t-KTN and bare Zn. Reprinted with permission.^[127] Copyright 2022, WILEY-VCH.

Raman spectroscopy analysis revealed that the LZS layer facilitated the tight binding of $[\text{Zn}^{2+}\text{SO}_4^{2-}]$ ion pairs and significantly altered the solvation structure of hydrated Zn^{2+} at the interface (Figure 10h). The energy barrier for the stepwise desolvation of $[\text{Zn}(\text{H}_2\text{O})_n]^{2+}$ at the LZS interfaces was investigated by a DFT computational system. At the untreated Zn/electrolyte interface, an energy barrier of 7.36 eV needs to be overcome for $[\text{Zn}(\text{H}_2\text{O})_6]^{2+}$ to desolvate water molecules. In comparison, only 5.31 eV is required at the Zn@LZS/electrolyte interface (Figure 10i). The lower energy barrier for desolvation facilitates the acceleration of Zn^{2+} diffusion kinetics. At 0.5 mA cm^{-2} , the LZS@Zn symmetric cell can provide ultra-low overpotential (23.2 mV) with 99.8% CE in 3300 cycles, which is stable even at low temperature ($>3600 \text{ h}$, 48.2 mV hysteresis) (Figure 10j). The Zn deposition process was observed in real time using an in situ optical microscope (Figure 10k). The thickness of the Zn layer deposited by LZS@Zn increased uniformly, and no obvious dendrites or H_2 bubbles were observed.

3.3.2. Non-oxide Inorganic Compounds

Inspired by lithium-based SEI for lithium metal anode protection, fluorinated inorganic compounds have been widely used for zinc anode

protection. Li et al. designed a 3D interconnected ZnF_2 array (Zn@ZnF_2) as a multifunctional protective layer (Figure 11a).^[132] The construction of the ZnF_2 coating not only redistributes the Zn^{2+} flux but also significantly reduces the desolvation activation energy barriers of hydrated zinc ions, which facilitates more stable Zn deposition. However, the ZnF_2 exhibits excessive internal resistance, which reduces the ion transport and increases the polarization voltage. This effect is particularly noticeable at high current densities. To alleviate this problem, adding a zincophilic metal to provide nucleation sites can effectively promote the deposition uniformity at high current densities. Yan et al. introduced the metal indium (In) to construct an ultrathin ZnF_2 -In interfacial layer (Figure 11b).^[133] The bilayer structure of ZnF_2 -In was confirmed by EDS and XRD (Figure 11c,d). The DRT analysis (Figure 11e) reveals that the accumulation of by-products at the bare Zn electrode hinders the Zn^{2+} desolvation kinetics. In contrast, the ZnF_2 -In@Zn electrode exhibits a stable and low impedance property. This excellent performance is attributed to the outer ZnF_2 layer, which facilitates the complete desolvation of $[\text{Zn}(\text{H}_2\text{O})_6]^{2+}$ and promotes homogeneous ionic flow, and the inner In layer, which optimizes the electric field distribution and reduces the nucleation barrier. The ZnF_2 -In interfacial layer enables dendrite-free and side-reaction-free zinc deposition, sustaining a stable cycling for over 2100 h at 5 mA cm^{-2}

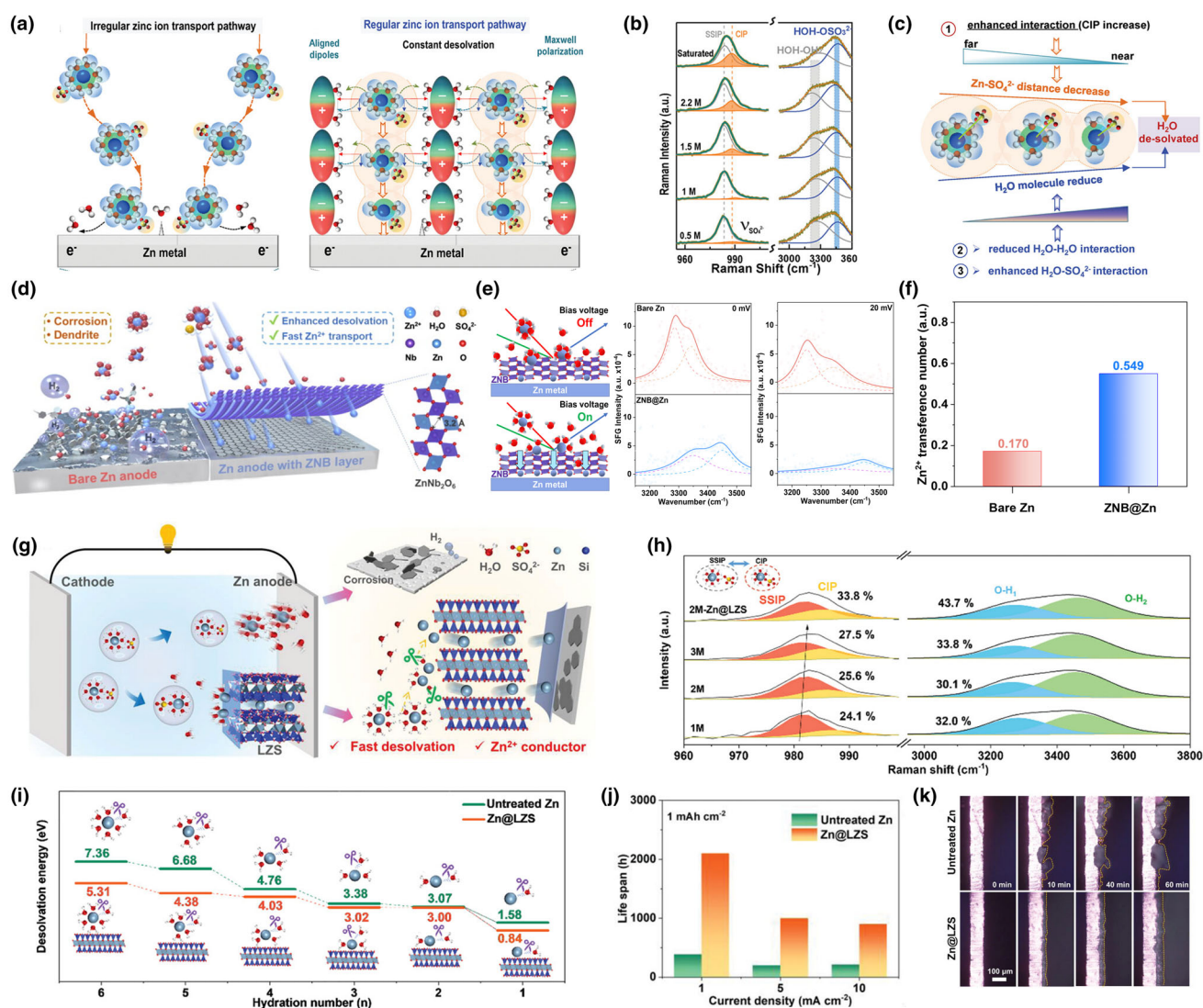


Figure 10. a) Schematic of Maxwell polarized electric field guided vertical Zn^{2+} deposition. b) Raman spectra of electrolytes under different concentrations. c) Schematic illustration of how electrolyte changes the charged IF-BTO layer. Reprinted with permission.^[129] Copyright 2023, WILEY-VCH. d) Schematic illustration of the Zn plating behavior with ZNB layer. e) SFG signal of $[\text{Zn}(\text{H}_2\text{O})_6]^{2+}$ at the interface with and without bias voltage. f) Zn^{2+} transference number of bare Zn and ZNB@Zn. Reprinted with permission.^[130] Copyright 2025, Elsevier. g) Schematic illustration of the Zn plating of LZS layer. h) Raman spectra of $\nu\text{-SO}_4^{2-}$ band and O-H band. i) Comparison of $[\text{Zn}(\text{H}_2\text{O})_6]^{2+}$ desolvation barriers with/without LZS layer. j) The summary of long-term galvanostatic charge/discharge performance at different current densities. k) In situ optical microscopic observation. Reprinted with permission.^[131] Copyright 2024, WILEY-VCH.

(Figure 11f). However, many fluorides are toxic, which conflicts with the intrinsic safety requirements of AZMBs. Therefore, researchers have started to explore non-toxic fluorides as alternative materials. Li et al. employed CaF_2 to construct an environmentally friendly artificial protective layer, which achieved uniform Zn^{2+} flux modulation and satisfied the green concept of safety and environmental protection.^[134] This CaF_2/Zn interfacial layer effectively controlled zinc deposition behavior, and the assembled symmetric cell exhibited an excellent cycling stability of up to 1850 h at a current density of 1 mA cm^{-2} .

Inorganic compounds incorporating sulfur (S),^[135] selenium (Se),^[136] nitrogen (N),^[137,138] and similar elements have also been utilized to engineer artificial interfacial protectants on the zinc anode. For instance, a dense ZnS layer fabricated in situ on the zinc metal

surface through a vapor-solid reaction significantly enhances reversibility by utilizing the firm adhesion of ZnS, high mechanical strength, and excellent ionic conductivity.^[135] DFT calculations reveal that interfacial charge transfer between ZnS and metallic Zn generates strong S-Zn bonds; the resulting charge imbalance accelerates Zn^{2+} transport across the ZnS@Zn interface and simultaneously reinforces the ZnS layer's binding to the underlying metal. In contrast, a mechanically resilient ZnSe coating grown directly on Zn foil through selenization creates a highly zincophilic barrier filled with ionic-diffusion channels.^[136] The ZnSe@Zn architecture exhibits an exceptional affinity for Zn and offers intrinsic pathways for rapid ion migration, thereby promoting uniform nucleation kinetics and accelerated charge/discharge dynamics. Symmetric cells equipped with

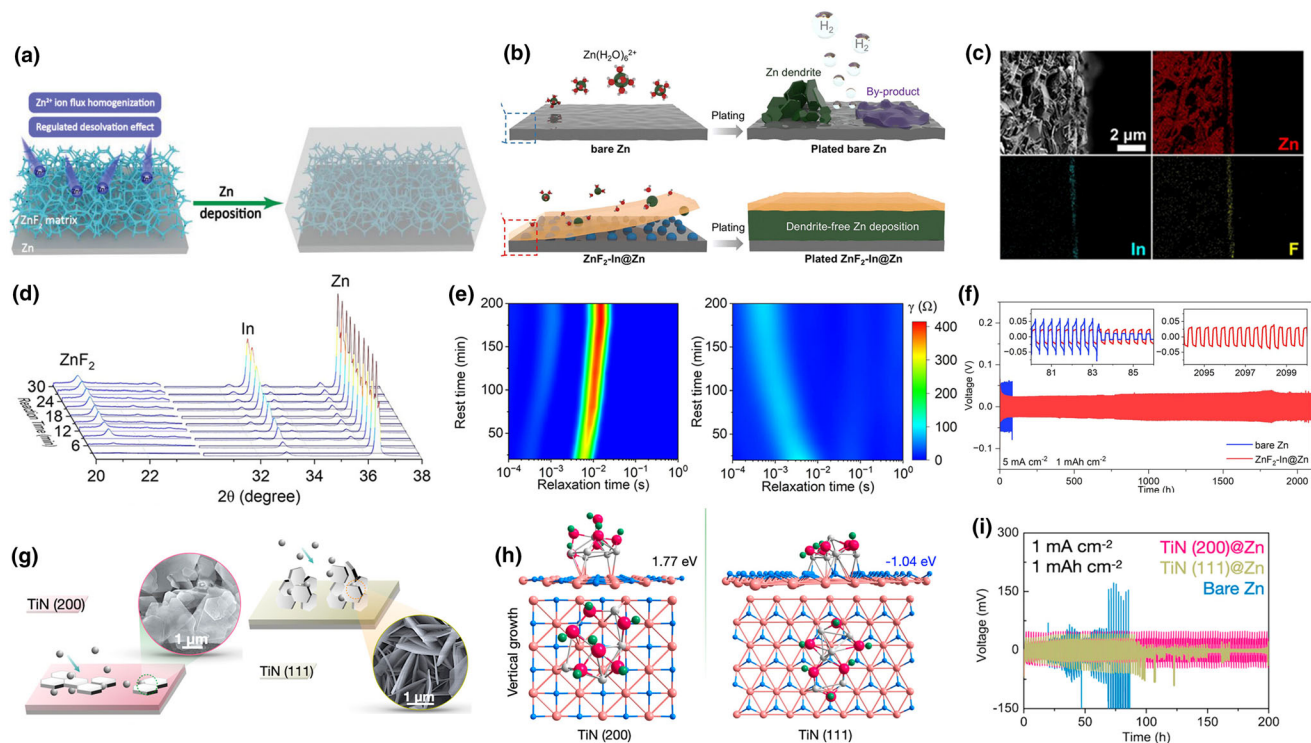


Figure 11. a) Schematic illustration of the fabrication of the Zn@ZnF₂ electrode. Reprinted with permission.^[132] Copyright 2021, WILEY-VCH. b) Schematic illustration of the Zn plating process on bare Zn and ZnF₂-In@Zn electrodes. c) Cross-sectional SEM image with EDS mapping of the ZnF₂-In@Zn electrode. d) XRD patterns of ZnF₂-In@Zn at different reaction times. e) DRT analysis of bare Zn and ZnF₂-In@Zn. f) Galvanostatic cycling of bare Zn and ZnF₂-In@Zn symmetric cells at 5 mA cm⁻². Reprinted with permission.^[133] Copyright 2024, American Chemical Society. g) Growth patterns of zinc hydroxide on TiN (200) and TiN (111) crystal faces. h) Simulation of zinc hydroxide sulfate deposition behavior on TiN coatings. i) Voltage curves for symmetrical cells at 1 mA cm⁻². Reprinted with permission.^[137] Copyright 2021, American Chemical Society.

ZnSe@Zn anodes deliver outstanding cyclability (>1700 h) across a wide range of areal capacities (0.2–5.0 mAh cm⁻²) and show minimal voltage hysteresis even at high rates. Moreover, a TiN protective film deposited on the Zn anode through magnetron sputtering effectively directs byproduct growth laterally, suppressing corrosion induced by hydrogen evolution.^[137] As illustrated in Figure 11g, simulations of ZHS deposition onto various TiN crystallographic facets indicate that the TiN (200) plane energetically favors planar ZHS growth. In contrast, the herringbone-structured TiN (111) surface thermodynamically induces pyramidal deposition (Figure 11h). This facet-selective behavior curtails HER-driven degradation, enabling the TiN-coated anode to sustain stable cycling for over 2300 h at 1 mA cm⁻² and 1 mAh cm⁻² (Figure 11i).

It is worth noting that the method of constructing inorganic material coatings on Zn electrodes is primarily the traditional squeegee method, in which inorganic materials are mixed with adhesives such as polyvinylidene fluoride (PVDF) through physical mixing. However, this method has several drawbacks. PVDF has been found to cause clogging of the pores of the porous material during the mixing process and create numerous tiny cracks during solvent evaporation. These factors have a detrimental effect on the mechanical stability of the coating. Additionally, this method results in disordered stacking of the coating, which increases the ion transfer path and enhances the charge transfer resistance. Therefore, exploring alternative preparation methods to build gapless and ultrathin inorganic material layers is the focus of future research.

3.4. Organic Compounds

Organic materials, renowned for their flexibility, porous structure, and tunable polar groups, are considered ideal candidates for various battery systems. The optimal organic coating material should achieve several properties: firstly, the interface should be ionically conductive while remaining electronically insulating. Secondly, the polymer coating should be dense and insoluble in the aqueous electrolyte. Third, the protective layer needs to be hydrophilic to facilitate the diffusion of ions through the coating. Finally, it should demonstrate strong adhesion to the zinc metal surface and possess good mechanical properties.^[139,140] Depending on the polymer matrix material, organic coatings applied to AZMB are categorized as non-porous organic polymers and porous organic polymers (including metal organic frameworks (MOFs) and covalent organic frameworks (COFs)).

3.4.1. Non-porous Organic Polymers

Non-porous organic polymer materials inherently lack pore structures. When employed as AILs to regulate Zn²⁺ transport, they require pore channels constructed via specific fabrication methods. Common non-porous organic polymers include polyamide (PA),^[141] polyvinyl butyral (PVB),^[142] polyvinyl alcohol (PVA), polyacrylonitrile (PAN),^[143] and polymethyl methacrylate (PMMA)^[144] etc. Firstly, the abundance of functional groups in these polymers can be utilized as

nucleation sites to induce the homogeneous deposition of Zn. The long-chain structure provides the coating with mechanical flexibility, ensuring its structural integrity during the cycling process. Secondly, the electronic insulating property of non-porous organic polymer materials can reduce the possibility of contact between active water and electrons, effectively delaying the formation of corrosion products on active sites through physical shielding, which slows down the passivation process. Cui et al. developed a multifunctional polymer interfacial layer composed of polyamide (PA) and zinc trifluoromethanesulfonate ($\text{Zn}(\text{TfO})_2$).^[141] The polyamide organic layer coordinates with metal ions through a unique hydrogen bonding network, which not only regulates the Zn^{2+} migration path but also promotes uniform nucleation of Zn. Further studies reveal that the introduction of polar groups is an effective strategy in improving the interfacial hydrophilicity. Wu et al. significantly enhanced the hydrophilicity of the material by reducing the contact angle at the electrolyte/electrode interface from 77.9° to 26.3° through the introduction of a linearly polar cyano group ($-\text{CN}$) into PAN.^[143] The improvement in wettability effectively reduced the resistance to ion transport at the interface, enabling Zn^{2+} to be distributed uniformly across the electrode surface. An insulating PMMA coating was designed by Lu et al.^[144] which not only inhibited the side reaction and protected the Zn anode but also enabled a stable Zn deposition process by binding Zn^{2+} through abundant zincophilic sites.

3.4.2. Porous Metal Organic Framework (MOFs)

MOFs are a class of scalable porous materials assembled by the coordination assembly of metal cation centers with organic ligands. MOFs are candidates for zinc anode AILs due to their enriched porous structure, abundant adjustable sites, and ultra-high specific surface area. On the one hand, the rich pore structure provides directional channels for Zn^{2+} transport and promotes uniform ion distribution. On the other hand, the polar functional groups (e.g., $\text{C}=\text{O}$, $-\text{NH}_2$) in the backbone can serve as zincophilic sites, reducing the nucleation barrier.^[145] In addition, the high specific surface area and porous structure of the MOF can buffer the volume change during charging and discharging, thereby maintaining the stability of the electrode during cycling. MOFs based on zeolite imidazolum hydrochloride framework (ZIF) (e.g., ZIF-7,^[146] ZIF-8^[147]) have an ordered porous structure, which can effectively promote the transport of Zn^{2+} while hindering the electron conduction. Taking ZIF-7 as an example, it promotes the desolvation of hydrated zinc-ion solvation sheaths.^[146] Schematic representations and Raman spectroscopy analyses reveal that under the influence of a 2.94 \AA pore window in ZIF-7 (Figure 12a), the relatively large $[\text{Zn}^{2+}(\text{H}_2\text{O})_6\text{SO}_4^{2-}]$ complex should shed a portion of its coordinated water molecules to form a monohydrated zinc complex capable of permeating the pore. During this process, the continuous reduction in water content engenders a supersaturated electrolyte at the interface, thereby mitigating dendritic growth induced by concentration polarization (Figure 12b–d).

Nonetheless, the inherently slow desolvation kinetics may compromise ion diffusion, rendering the Zn^{2+} plating/stripping process unstable at higher current densities. Incorporating polar functional groups to enhance local electrolyte enrichment has emerged as an effective strategy to address this challenge. In this context, Zhu et al. introduced carboxyl ($-\text{COOH}$) groups into a zirconium-based MOF (UiO-66) to improve ion transfer efficiency during Zn^{2+} desolvation (Figure 12e), thereby achieving stable zinc deposition even under high current densities.^[148] Comparison of Raman spectra of UiO-66@Zn and $\text{UiO-66-(COOH)}_2\text{@Zn}$

after cycling showed that the carboxyl-functionalized $\text{UiO-66-(COOH)}_2\text{@Zn}$ exhibited a significantly enhanced SO_4^{2-} absorption peak at 998 cm^{-1} , which proved the better electrolyte enrichment within the pores (Figure 12f,g). This observation is partially attributed to the increased contact angle between the electrode and water resulting from carboxyl group incorporation (Figure 12h). Moreover, owing to its high hydrophilicity, UiO-66-(COOH)_2 attains an ionic conductivity of up to 1.91 mS cm^{-1} (Figure 12i), thereby facilitating rapid Zn^{2+} transfer and accelerating electrolyte diffusion.

3.4.3. Covalent Organic Framework (COFs)

COFs represent an emerging class of organic crystalline porous materials made of organic compounds.^[149] They have regular structures and clearly defined pore designs, which provide organized pathways for ion transport. Meanwhile, their adjustable functional groups, such as $\text{C}=\text{O}$, $\text{C}=\text{N}$, $-\text{F}$, and $-\text{NH}_2$, allow for specific interactions with anions, cations, and solvent molecules, facilitating the separation of metal ions in the electrolyte.^[150,151] Lan et al. designed a zincophilic COF (Zn-AAAn-COF) protective layer that can be synergistically regulated by the precipitation of hydrogen and the flux of zinc ions.^[152] DFT calculations showed that the adsorption energy of Zn-AAAn-COF on Zn atoms was higher than that of Zn foils, suggesting that Zn-AAAn-COF had a better Zn affinity. The spatial electrostatic potential effect constructed by modifying Zn foils with Zn-AAAn-COF can reduce the desolvation energy barrier of hydrated Zn^{2+} and alleviate hydrogen precipitation corrosion. Additionally, the homogeneous pore structure facilitates the uniform distribution of Zn^{2+} flux, thereby inhibiting the growth of dendrites. Superhydrophobic perfluorinated chain-modified covalent organic frameworks (SPCOFs) were employed by Luo et al.^[153] The introduction of $-\text{F}$ serves to reduce the surface energy of the nanochannels, thereby regulating the interaction between the electrolyte solution and the channel walls. This process accelerates the process of dehydration. The dehydrated Zn solvent sheath layer detaches from the channel wall, occupying a larger central region within the unwetted nano-channel. The dehydrated Zn^{2+} diffuses rapidly in the unwetted channel, lowering the migration energy barrier. By carefully designing the framework structure, the ion migration paths within the SPCOF channels can be optimized to promote fast ion transport and stable zinc deposition. Stable cycling for 5000 h at a high current density of 10 mA cm^{-2} significantly improved the stability and lifespan of the cell. Lan et al. also employed anhydride-based COFs with unique sawtooth jumping sites (PI-DP-COFs) as AILs to guide the transport behavior of Zn^{2+} inside the AILs.^[154] The ABC stacking mode of PI-DP-COFs resulted in a staggered node arrangement. Molecular dynamics simulations reveal that the large number of $\text{C}=\text{O}$ and $\text{C}=\text{N}$ sites in the protective layer of PI-DP-COF facilitates the rapid jumping and migration of Zn^{2+} . DFT theoretical calculations indicate that the structure can effectively mitigate the solvation effect of hydrated zinc ions, thereby inhibiting the HER.

A distinct type of COFs is ionic COFs (iCOFs),^[155,156] which are COFs that contain a repeating unit bearing ionic groups. In this regard, iCOFs can be compared to polyelectrolytes because a significant number of the groups in their polymer backbones are ionic or ionizable. iCOFs retain the atomic structure and natural porosity of original COF designs while integrating charged groups either within the framework or as side-chain features. This combination thereby enhances their versatility by providing several benefits. Chen et al. used in situ electrophoretic deposition (ED) to develop an iCOF with a porous structure and numerous zincophilic sites.^[157] The porous structure and numerous

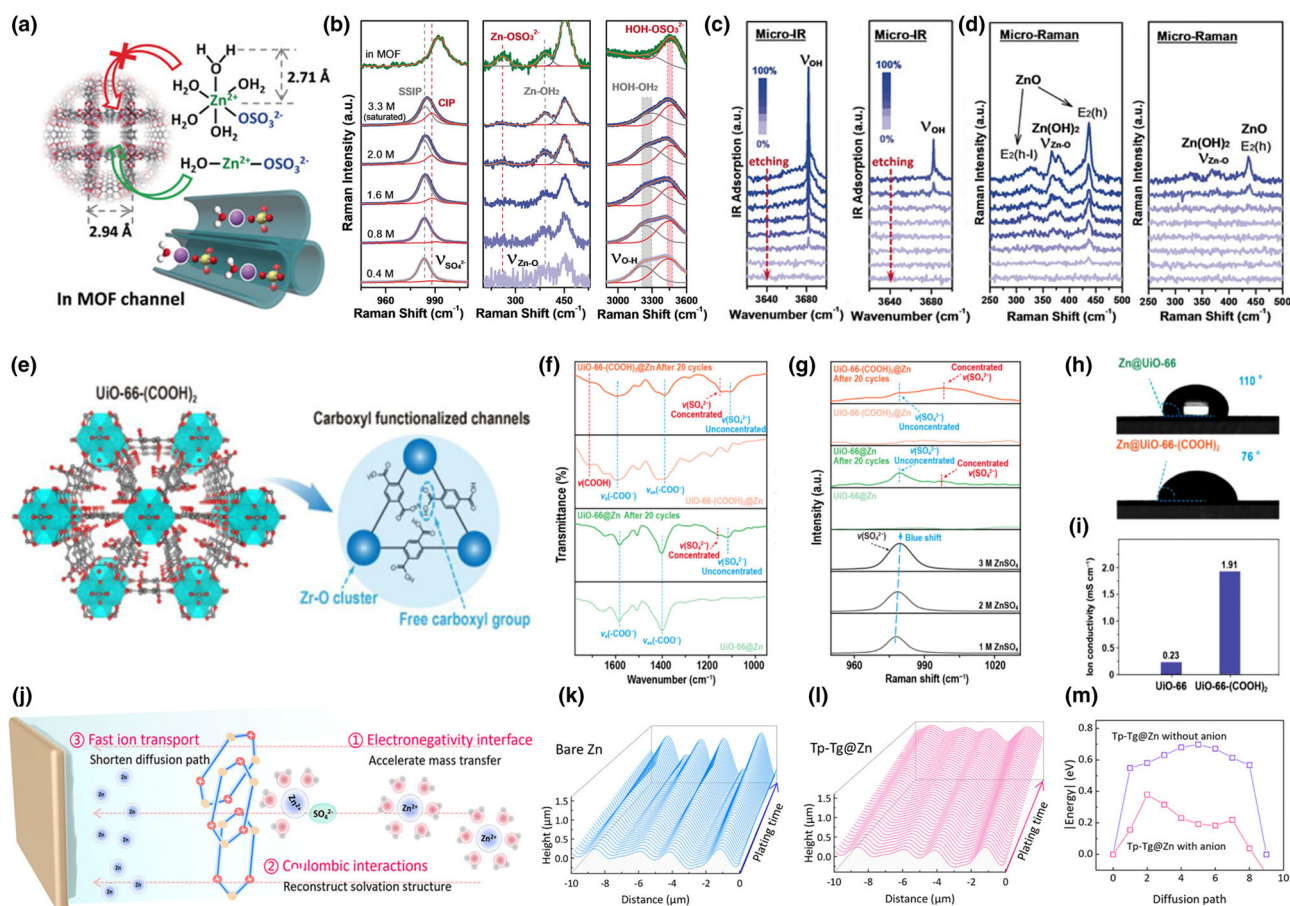


Figure 12. a) Schematic illustration of highly coordinated ion complexes of $\text{H}_2\text{O}-\text{Zn}^{2+}-\text{OSO}_3^{2-}$ migrating through MOF channels. b) Raman spectroscopy of concentration gradient ZnSO_4 aqueous solutions and in MOF channels. c, d) Micro-IR and Micro Raman spectroscopy of bare Zn and MOF-coated Zn anodes. Reprinted with permission.^[146] Copyright 2020, WILEY-VCH. e) Schematic illustration of the functional mechanism of the UiO-66-(COOH)₂ coating layer for protecting the Zn anode. f, g) FT-IR spectra and Raman shift spectroscopy of UiO-66@Zn and UiO-66-(COOH)₂@Zn before and after 20 cycles. h) Contact angle of electrolyte on the UiO-66@Zn and UiO-66-(COOH)₂@Zn. i) Ion conductivity of UiO-66 and UiO-66-(COOH)₂. Reprinted with permission.^[148] Copyright 2023, Elsevier. j) Schematic illustration of distinct Zn^{2+} transport behaviors on Tp-Tg@Zn. k, l) Growth trends of Zn deposition morphology over time on bare Zn and Tp-Tg@Zn. m) Energy diagrams of Zn^{2+} migration between COF layers with/without anion. Reprinted with permission.^[150] Copyright 2025, WILEY-VCH.

zincophilic sites allow for a consistent flow of Zn^{2+} and rapid desolvation, facilitating efficient mass and charge transfer, which leads to stable and uniform Zn^{2+} deposition. Sun et al. reported a multifunctional Tp-Tg iCOF interfacial membrane developed on commercial zinc foil (Tp-Tg@Zn) to regulate Zn^{2+} transport and enhance the durability of zinc anodes (Figure 12j).^[150] On the one hand, the unmodified Zn anode interface suffers from severe Zn^{2+} depletion due to rapid reduction kinetics, while the negatively charged Tp-Tg modified interface maintains a stable electrostatic environment that promotes uniform Zn^{2+} distribution (Figure 12k,l). Crucially, this stable environment arises from the Coulombic interaction between the positively charged skeleton and SO_4^{2-} encourages the dissociation of Zn^{2+} , thereby reducing the diffusion energy barrier of Zn^{2+} . This interaction reduces the diffusion energy barrier of Zn^{2+} within the Tp-Tg layer, facilitating stable ion movement and uniform zinc deposition (Figure 12m). As a result of these mechanisms, the 20 μm Zn anode coated with the Tp-Tg layer achieved stable cycling for 300 h under harsh conditions (1.0 mA cm^{-2} /10.0 mAh cm^{-2} , 50% DOD).

Currently, strategies such as defect engineering, small molecules incorporation, or the addition of short-chain polymers can effectively reduce the migration energy barrier for Zn^{2+} in COFs by enhancing ion solvation and transport. Future research should investigate a wider range of methods to create a comprehensive design framework for the development of advanced zinc metal batteries using COF materials that exhibit long-term cycling stability and high reversibility.

In comparison to organic SEIs formed in situ through electrolyte engineering, artificially constructed organic SEIs provide more complete and uniform coverage on the zinc metal anode surface, providing more comprehensive protection for the anode. Therefore, organic AILs offer significant advantages in stabilizing zinc negative electrodes. However, currently reported organic materials exhibit issues such as entangled molecular chains, non-uniform pore structure distribution, and structural degradation during long-term cycling, which impede the development of anode protective layers.^[158] In order to address current challenges, the future development of organic AILs should focus on the selection of organic materials, the design of pore structures, and the

regulation of functional groups in molecular chains. Specifically, the concurrent design of organic polymer coatings and electrolyte engineering allows for the creation of artificial organic SEIs that are stabilized through electrolyte engineering. This mitigates issues such as coating degradation and achieves organic AILs with “self-healing” functionality.

4. Conclusion and Outlooks

In conclusion, the construction of AILs on zinc metal surface represents an effective strategy to address the issues of dendrite growth, HER, and side reactions. While various materials can regulate Zn^{2+} deposition behavior and improve cycling stability, the advantages and limitations of each should be comprehensively evaluated as an essential part of commercial feasibility assessment. In this review, the various materials used for constructing AILs are systematically discussed, including carbon materials, zincophilic alloys, and inorganic/organic materials. A critical analysis of each material category is presented to provide a reference basis for the design of programmable AILs.

As mentioned in this review, carbon materials with high electrical conductivity can reduce interfacial impedance and facilitate zinc-ion transport. The large specific surface area can lower the local current density and induce uniform Zn^{2+} deposition. Nevertheless, when carbon materials are used as Zn coatings, the excellent conductivity may be unfavorable for zinc-ion deposition. The Zn^{2+} tends to deposit on the coating surface rather than on the zinc metal surface, which leads to dendrite growth and HER on the Zn anode surface. Zincophilic alloys can directly modify the zinc metal, providing nucleation sites, refining grains, and reducing grain boundary corrosion. However, due to the structural heterogeneity of exogenous metals, the exogenous metals can impact the durability of the interface, thereby disrupting long-term plating/stripping. Inorganic compounds can precisely regulate the migration pathways of charge carriers through their porous structures and isolate direct contact between active water molecules and the electrode. Some inorganic compound materials can also generate local electric fields via spontaneous polarization effects, thereby significantly enhancing zinc-ion transport kinetics. But, they are generally regarded as inert protective layers with no electrochemical reactivity, and excessive coating thickness will reduce the energy density of AZMBs. Organic materials are rich in functional groups that can interact with Zn^{2+} , promoting uniform zinc deposition and exhibit high hydrophilicity and efficient ion transport. Despite these advantages, the organic materials reported so far face issues such as molecular chain entanglement, non-uniform pore structure distribution, and structural degradation during long-term cycling.

To effectively address challenges faced by zinc metal anodes during cycling and significantly enhance the CE and cycling stability of AZMBs, more in-depth and systematic research is essential. Regarding AILs' design should consider not only material composition but also practical factors encountered during application. These include the construction techniques of AILs, regulation of hydrophilicity and hydrophobicity, optimization of AIL thickness, and the structural design of composite and self-healing AILs. Meanwhile, to improve the performance of AZMBs, it is crucial to conduct more detailed tracking and characterization of in situ electrochemical reaction dynamics at the electrode/electrolyte interface. This approach will help reveal the fundamental kinetics of zinc nucleation and growth while providing theoretical guidance to ensure the long-term stability of the zinc anode, enhance energy density, and enable reliable operation under extreme

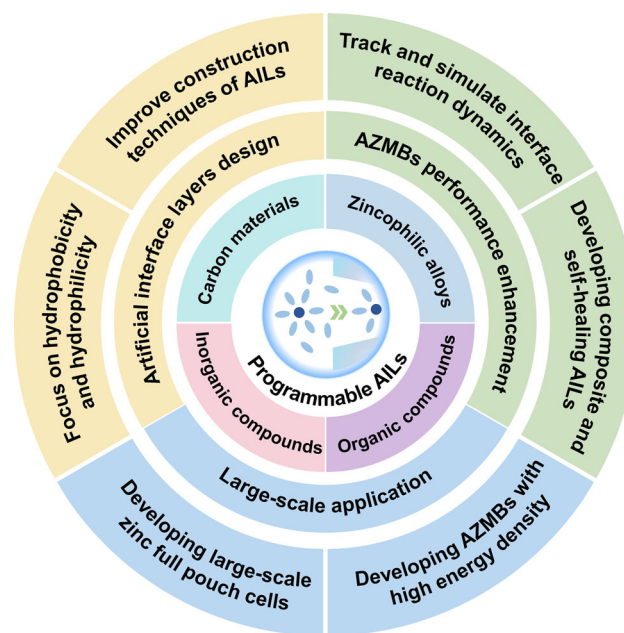


Figure 13. The targets and outlooks for the development of AILs and practical AZMBs.

conditions. In the future, the research focus for AZMBs should gradually shift from laboratory-scale coin cells to the scalable production of pouch cells, alongside establishing a more systematic research framework to lay a solid foundation for commercialization. Based on the above analysis, several development recommendations are proposed (Figure 13), aiming at promoting the practical application of AZMBs and meeting the requirements of large-scale applications.

4.1. Improve Construction Techniques of AILs

At present, the techniques for construction AILs are primarily categorized into in situ synthesis and ex-situ synthesis. In situ synthesized AILs demonstrate superior Zn^{2+} transport capability and stability. Their fabrication often requires complex conditions. In contrast, ex-situ synthesis methods are simpler, but tend to produce coatings that are more prone to delamination. Additionally, the thickness of the coating has a significant impact on battery performance. The low thickness of coatings can decrease the Zn^{2+} diffusion distance and reduce migration resistance, thereby improving battery rate capability. However, reducing the thickness of the coating could compromise its mechanical properties, posing a risk to long-term cycling stability. Current strategies often increase the coating thickness to enhance mechanical strength and toughness, which helps maintain the structural integrity of the AIL during operation. Future efforts should focus on developing more advanced and convenient AIL fabrication techniques that balance coating thickness with cycling stability, ion transport efficiency, and rate performance.

4.2. Focus on Hydrophobicity and Hydrophilicity of AILs

There are two perspectives on whether coating design strategies should focus on enhancing hydrophilicity or hydrophobicity: 1) some research

focuses on enhancing coating hydrophilicity by incorporating abundant hydrophilic groups (e.g., -OH, -F, -COOH). These hydrophilic group-rich coatings are believed to interact with hydrated zinc ions, facilitating their partial desolvation and enabling rapid transport through the coating, thereby increasing the Zn^{2+} transference number. 2) Some studies focus on developing hydrophobic but zincophilic AILs. The main idea is to decrease the contact between the electrode/electrolyte to reduce side reactions. However, the increased coating hydrophobicity typically leads to reduced wettability, elevated interfacial impedance, and potentially aggravated zinc dendrite growth. Thus, this strategy focuses on including abundant zincophilic groups within the hydrophobic structure to promote uniform zinc-ion flux. In practice, regardless of whether the coating design focuses on enhanced hydrophilicity or hydrophobicity, the main objective is to ensure uniform and rapid Zn^{2+} transport on the electrode interface and effectively suppress water decomposition. Future coating design efforts should aim to improve the Zn^{2+} transport kinetics to achieve a uniform and stable zinc deposition process.

4.3. Develop Composite and Self-Healing AILs

To simultaneously inhibit dendrite growth and side reactions and achieve multiple protection for zinc electrodes, the selection of materials for AIL should satisfy various performance requirements. One of the possible directions is the development of hybrid materials that combine the advantages of conductive and insulating materials. This multiphase composite coating can be designed with a gradient multilayer structure: 1) the inner conductive-electronic layer regulates the interfacial charge distribution; 2) the intermediate transition layer provides mechanical stability to the coating; 3) the outer conductive-ionic layer serves as an electronic barrier, screening the passage of ions of specific sizes. This multiphase complex coating design improves mechanical stability, ionic conductivity, and cycling stability. In the future, it is necessary to develop materials with self-adaptive and self-repairing functions, which can automatically repair coating deformation damage during battery cycling, thereby further enhancing the cycle lifespan and safety of the battery.

4.4. Track and Simulate in Situ Interface Electrochemical Reaction Dynamics

Although the effect of deposition behavior on cycle lifespan has received considerable attention from researchers, the microscopic reaction mechanisms at the electrode/electrolyte interface remain insufficiently investigated. Currently, theoretical models of the zinc anode interface are largely based on previous studies such as lithium, sodium, and alkali metal anodes. However, the electrode/electrolyte interface of zinc anodes in aqueous electrolytes differs significantly from that of lithium or sodium anodes in organic electrolytes, and the morphology of zinc dendrites also differs from other alkali metal anodes. Therefore, there is an urgent need to integrate more experimental studies, simulations, and theoretical calculations to deepen the understanding of zinc nucleation and growth mechanisms, including SFG, in situ transmission electron microscopy (in situ TEM), in situ Raman spectroscopy, in situ XPS, in situ X-ray absorption spectroscopy, and in situ mass spectrometry (MS). These approaches will provide reliable dynamic data, helping to reveal the fundamental mechanisms of interfacial reactions and

deepen the understanding of zinc plating/stripping behaviors. At the same time, future studies should develop theoretical models integrated with a variety of characterization techniques to achieve a more comprehensive investigation of Zn^{2+} transport in the interphase layer. At the atomic scale, DFT and ab initio molecular dynamics can precisely calculate the migration energy barriers and adsorption properties of Zn^{2+} in different structural units. At the molecular scale, molecular dynamics simulations can elucidate diffusion coefficients, solvation shell structures, and their dynamic reorganization. At the macroscopic scale, finite element analysis can be applied to describe concentration gradients, electric field distributions, and transport morphology evolution. Moreover, integrating multiscale simulations with machine learning and in situ characterization techniques will provide mechanistic guidance for optimizing the structure of AILs, promoting the development of AZMBs with higher energy density and longer cycle lifespan.

4.5. Develop AZMBs with High Energy Density

The zinc anode is particularly attractive due to its high theoretical gravimetric and volumetric capacities (820 mAh g^{-1} and 5855 mAh cm^{-3}). However, in current studies, thick zinc foils ($\geq 100 \mu\text{m}$) are usually used as anodes. The excess zinc can be continuously replenished to counteract the losses caused by “dead Zn” and side reactions.^[159,160] This approach leads to low utilization of zinc anodes and squanders the high energy density of AZMBs. To enhance the anode energy density, the primary strategy is to reduce the amount of zinc metal, which can be achieved through methods such as thinning the zinc foil, employing pre-deposited zinc metal anodes, or adopting anode-free zinc metal batteries.^[161] Additionally, optimizing separators can further improve energy density by reducing separator thickness while maintaining mechanical integrity. On the cathode side, the main strategies include increasing cathode capacity or loading and minimizing the mass and volume of current collectors by adjusting their 3D architecture. Nevertheless, excessively thick cathodes can suffer from sluggish ion transport kinetics and increased impedance, ultimately reducing cathode utilization. Future research should focus on developing thick electrodes with superior ion diffusion properties or exploring novel cathode materials with higher specific capacities to meet practical application requirements.

4.6. Develop Large-Scale Zinc Metal-Based Full Pouch Cells for Commercialization Applications

The development of AZMBs offers broad prospects for the sustainable advancement of energy storage. Although they have been extensively studied and validated in laboratories, numerous challenges remain in translating these results into practical applications. A key factor lies in fully recognizing the significant differences between laboratory testing conditions and real-world operating scenarios. At present, most research focuses on coin cells, while studies on pouch cells are still insufficient. It should be noted that scaling up battery size often exacerbates the issues encountered in coin cells. It is necessary to systematically evaluate performance differences under different testing conditions and establish a consistent, comprehensive testing standard to facilitate the transition of AZMBs from fundamental research to commercialization applications. Future works should focus on the synergistic optimization of all battery components, such as the co-regulation of

ALLs and electrolyte engineering, to optimize zinc deposition behavior, ion transport dynamics, improve cycle lifespan, and cycle stability. Furthermore, modular design and tailored adaptation to specific application scenarios will play a crucial role in advancing the commercialization of AZMBs.

Acknowledgements

We acknowledge National Key Research and Development Program of China (2021YFA1201503); the National Natural Science Foundation of China (Nos. 225722217, 1972164, 12264038, and 22309144), China Postdoctoral Science Foundation (Nos. 2024M762318, 2023M731084, and 2023M732561), Jiangsu Provincial Science and Technology Program (Major Project) (No. BG 2024020), Opening funding from Key Laboratory of Engineering Dielectrics and Its Application (Harbin University of Science and Technology) (No. KFM202507, Ministry of Education), Guangdong Basic and Applied Basic Research Foundation (No. 2024A1515110244), as well as the technical support from Nano-X, Suzhou Institute of Nano-tech and Nano-bionics, Chinese Academy of Sciences. Dr. J. Wang thanks the funding provided by the Alexander von Humboldt Foundation. Open Access funding enabled and organized by Projekt DEAL.

Conflict of interest

The authors declare no conflict of interest.

Data Availability Statement

No primary research results, software or code have been included and no new data were generated or analyzed as part of this review.

Keywords

aqueous zinc metal batteries, artificial layer, programmable construction, Zn anode protection, Zn dendrites

Received: July 30, 2025

Revised: September 9, 2025

Published online: September 12, 2025

- [1] J. Zhang, C. You, H. Lin, J. Wang, *Energy Environ. Mater.* **2022**, 5, 731.
- [2] J. Xu, X. Cai, S. Cai, Y. Shao, C. Hu, S. Lu, S. Ding, *Energy Environ. Mater.* **2023**, 6, e12450.
- [3] C. Li, X. Xie, S. Liang, J. Zhou, *Energy Environ. Mater.* **2020**, 3, 146.
- [4] Z. Wu, F. Ye, Q. Liu, R. Pang, Y. Liu, L. Jiang, Z. Tang, L. Hu, *Adv. Energy Mater.* **2022**, 12, 2200654.
- [5] S. Kim, S. Woo, S. Byun, H. Kim, H. S. Kim, S. M. Jeong, D. Lee, *Energy Environ. Mater.* **2025**, 8, e12857.
- [6] H. S. Jeong, D. I. Kim, W. Lee, H. B. Jeong, S. Jo, J. Byeon, Y. Kwon, Y. Choi, W. B. Lee, S. Cha, J. P. Hong, J. I. Sohn, Y. Kim, J. Hong, *Energy Environ. Mater.* **2025**, 8, e12872.
- [7] J. Wang, J. Zhang, S. Duan, T. Li, L. Jia, H. Liu, L. Li, S. Cheng, H. Hu, M. Huang, H. Hu, S. Zhang, Q. Xiao, H. Lin, *Chem. Eng. J.* **2022**, 429, 132352.
- [8] J. Wang, H. Liu, J. Zhang, Q. Xiao, C. Wang, Y. Zhang, M. Liu, Q. Kang, L. Jia, D. Wang, Q. Li, W. Duan, H. Adenusi, S. Passerini, Y. Zhang, H. Lin, *Energy Storage Mater.* **2024**, 67, 103289.
- [9] J. Wang, L. Li, H. Hu, H. Hu, Q. Guan, M. Huang, L. Jia, H. Adenusi, K. V. Tian, J. Zhang, S. Passerini, H. Lin, *ACS Nano* **2022**, 16, 17729.
- [10] Y. Zhang, Z. Cao, S. Liu, Z. Du, Y. Cui, J. Gu, Y. Shi, B. Li, S. Yang, *Adv. Energy Mater.* **2022**, 12, 2103979.
- [11] J. Gu, Y. Tao, H. Chen, Z. Cao, Y. Zhang, Z. Du, Y. Cui, S. Yang, *Adv. Energy Mater.* **2022**, 12, 2200115.
- [12] J. Dong, X. Cheng, H. Yang, H. Li, H. Liu, L. Jia, Y. Zhang, Q. Guan, J. Jia, F. Wu, J. Zhang, M. Liu, H. Lin, J. Wang, *Adv. Mater.* **2025**, 37, 2501079.
- [13] H. Shi, J. Zheng, T. Wan, H. Wang, Z. Wen, F. Zheng, M. Su, A. Dou, *J. Energy Chem.* **2025**, 101, 392.
- [14] Y. Zhang, X. Li, Y. Wang, J. Zhu, Y. Zuo, X. Cheng, T. Rong, J. Zhang, Y. Hu, H. Lin, J. Wang, L. Zhan, L. Ling, *Adv. Funct. Mater.* **2025**, 35, 2508225.
- [15] Y. Lin, J. Wang, X. Zhang, X. Cheng, Q. Zhuang, J. Zhang, Q. Guan, Y. Wang, C. Shen, H. Lin, L. Zhan, L. Ling, Y. Zhang, *Adv. Funct. Mater.* **2025**, 35, 2501496.
- [16] J. Wang, J. Zhang, Y. Zhang, H. Li, P. Chen, C. You, M. Liu, H. Lin, S. Passerini, *Adv. Mater.* **2024**, 36, 2402792.
- [17] L. Sun, B. Zheng, W. Liu, *J. Colloid Interface Sci.* **2025**, 679, 197.
- [18] J. Wang, J. Zhang, J. Wu, M. Huang, L. Jia, L. Li, Y. Zhang, H. Hu, F. Liu, Q. Guan, M. Liu, H. Adenusi, H. Lin, S. Passerini, *Adv. Mater.* **2023**, 35, 2302828.
- [19] J. Wang, H. Hu, J. Zhang, L. Li, L. Jia, Q. Guan, H. Hu, H. Liu, Y. Jia, Q. Zhuang, S. Cheng, M. Huang, H. Lin, *Energy Storage Mater.* **2022**, 52, 210.
- [20] C. Wang, R. Li, Y. Zhu, Y. Wang, Y. Lin, L. Zhong, H. Chen, Z. Tang, H. Li, F. Liu, C. Zhi, H. Lv, *Adv. Energy Mater.* **2024**, 14, 2302495.
- [21] Q. Guan, J. Wang, Q. Zhuang, J. Zhang, L. Li, L. Jia, Y. Zhang, H. Hu, H. Hu, S. Cheng, H. Zhang, H. Li, M. Liu, S. Wang, H. Lin, *Energy Environ. Sci.* **2024**, 17, 3765.
- [22] J. Zhang, R. He, L. Jia, C. You, Y. Zhang, M. Liu, N. Tian, H. Lin, J. Wang, *Adv. Funct. Mater.* **2023**, 33, 2305674.
- [23] D. I. Kim, H. B. Jeong, J. Lim, H. S. Jeong, M. K. Kim, S. Pak, S. Lee, G.-H. An, S.-S. Chee, J. P. Hong, S. Cha, J. Hong, *Energy Environ. Mater.* **2025**, 8, e12826.
- [24] Y. Song, X. Wang, C. Liu, K. Guo, X. Guo, X. Zhong, Y. Zhang, K. Wang, H. Guo, L. Zhang, J. Liang, *Rare Metals* **2024**, 43, 3692.
- [25] X. Zhang, Y. Chen, C. Lin, Y. Lin, G. Hu, Y. Liu, X. Xue, S. Chen, Z. Yang, B. Sa, Y. Zhang, *Rare Metals* **2024**, 43, 3735.
- [26] B. Xu, Q. Li, Y. Liu, G. Wang, Z. Zhang, F. Ren, *Rare Metals* **2024**, 43, 1599.
- [27] Y. Yuan, S. Wu, X. Song, J. Y. Lee, B. Kang, *Energy Environ. Mater.* **2024**, 7, e12632.
- [28] Y. Cao, S. Ju, Q. Zhang, K. Gao, A. Marcelli, Z. Zhang, *Adv. Powder Mater.* **2025**, 4, 100278.
- [29] L. Jia, H. Hu, X. Cheng, H. Dong, H. Li, Y. Zhang, H. Zhang, X. Zhao, C. Li, J. Zhang, H. Lin, J. Wang, *Adv. Energy Mater.* **2024**, 14, 2304010.
- [30] D. Wang, Q. Li, Y. Zhao, H. Hong, H. Li, Z. Huang, G. Liang, Q. Yang, C. Zhi, *Adv. Energy Mater.* **2022**, 12, 2102707.
- [31] Y. Zhang, Z. Hu, Y. Bi, S. Tian, H. Sun, K. Li, W. Liu, L. Sun, W. Liu, D. Wang, *ACS Sustain. Chem. Eng.* **2025**, 13, 5381.
- [32] Q. Zhang, Y. Su, Z. Shi, X. Yang, J. Sun, *Small* **2022**, 18, 2203583.
- [33] X. Cheng, J. Dong, H. Yang, X. Li, X. Zhao, B. Chen, Y. Zhang, M. Liu, J. Wang, H. Lin, *Mater. Rep. Energy* **2025**, 5, 100313.
- [34] T. Li, A. Naveed, J. Zheng, B. Chen, M. Jiang, B. Liu, Y. Zhou, X. Li, M. Su, R. Guo, J. Sumner, C. C. Li, Y. Liu, *Angew. Chem. Int. Ed.* **2025**, 64, e202424095.
- [35] H. Wu, H. Yin, H. Tian, J. Yang, R. Liu, *Energy Environ. Mater.* **2025**, 8, e12839.
- [36] S. Deng, B. Xu, J. Zhao, H. Fu, *Energy Storage Mater.* **2024**, 70, 103490.
- [37] Y. Zhang, H. Zhou, J. Gu, H. Yang, X. Cheng, J. Zhang, J. Wang, Y. Wang, H. Lin, J. Wang, L. Zhan, L. Ling, *Energy Storage Mater.* **2025**, 76, 104161.
- [38] H. Ma, H. Chen, M. Chen, A. Li, X. Han, D. Ma, P. Zhang, J. Chen, *Nat. Commun.* **2025**, 16, 1014.

- [39] Z. Zhang, Y. Li, X. Yin, S. Li, B. Li, N. Zhao, J. Zhu, L. Dai, L. Wang, Z. He, Z. Feng, *Green Energy Environ.* **2025**, DOI: [10.1016/j.gee.2025.03.010](https://doi.org/10.1016/j.gee.2025.03.010).
- [40] K. Zhu, L. Wu, C. Guo, J. Pu, Y. Liu, X. Chen, Y. Chen, P. Xue, J. Han, Y. Yao, *Adv. Funct. Mater.* **2023**, 33, 2305098.
- [41] S. Liu, Q. Han, C. He, Z. Xu, P. Huang, L. Cai, H. Chen, H. Zheng, Y. Zhou, M. Wang, H. Tian, W. Q. Han, H. Ying, *ACS Nano* **2024**, 18, 25880.
- [42] W. Li, L. Li, X. Fu, Y. Hu, Y. Deng, *Small* **2025**, 21, 2411915.
- [43] C. Yang, P. Woottapanit, S. Geng, R. Chanajaree, K. Lolupiman, W. Limphiriat, X. Zhang, J. Qin, *ACS Energy Lett.* **2025**, 10, 337.
- [44] Z. Guo, Z. Liu, Y. Zhang, H. Li, M. Qi, C. Zhao, X. Zhang, Z. Wu, J. Yuan, N. Zhang, *Matter* **2025**, DOI: [10.1016/j.matt.2025.102269](https://doi.org/10.1016/j.matt.2025.102269).
- [45] X. Guo, S. Zhang, H. Hong, S. Wang, J. Zhu, C. Zhi, *iScience* **2025**, 28, 111751.
- [46] Z. Chen, R. Jiang, Y. Chen, H. Zhu, X. Tang, X. Huang, Y. Xie, J. Li, C. Zhang, L. Chen, W. Wei, L. Zhou, *Energy Storage Mater.* **2025**, 74, 103913.
- [47] R. Jiang, T. Naren, Y. Chen, Z. Chen, C. Zhang, Y. Xie, L. Chen, Y. Qi, Q. Meng, W. Wei, L. Zhou, *Adv. Funct. Mater.* **2024**, 34, 2411477.
- [48] D. Wang, D. Lv, H. Peng, C. Wang, H. Liu, J. Yang, Y. Qian, *Angew. Chem. Int. Ed.* **2023**, 62, e202310290.
- [49] H. Ji, Y. Liang, T. Yang, H. Wu, O. Sheng, T. Shen, C. Dong, T. Du, L. Yin, J. Zhang, R. Zheng, X. Zhang, *J. Mater. Sci. Technol.* **2026**, 240, 56.
- [50] S. Yang, G. Wu, J. Zhang, Y. Guo, K. Xue, Y. Zhang, Y. Zhu, T. Li, X. Zhang, L. Zhou, *Adv. Sci.* **2024**, 11, 2403513.
- [51] X. Yu, M. Chen, J. Wang, S. Li, H. Zhang, Q. Zhao, H. Luo, Y. Deng, H. Liang, J. Zhou, F. Wang, D. Chao, Y. Zou, G. Feng, Y. Qiao, S. G. Sun, *Nat. Commun.* **2025**, 16, 3820.
- [52] J. Wang, H. Hu, L. Jia, J. Zhang, Q. Zhuang, L. Li, Y. Zhang, D. Wang, Q. Guan, H. Hu, M. Liu, L. Zhan, H. Adenusi, S. Passerini, H. Lin, *InfoMat* **2024**, 6, e12558.
- [53] X. Zhao, Y. Wang, C. Huang, Y. Gao, M. Huang, Y. Ding, X. Wang, Z. Si, D. Zhou, F. Kang, *Angew. Chem. Int. Ed.* **2023**, 62, e202312193.
- [54] D. Chao, S.-Z. Qiao, *Joule* **2020**, 4, 1846.
- [55] B. Li, Y. Zeng, W. Zhang, B. Lu, Q. Yang, J. Zhou, Z. He, *Sci. Bull.* **2024**, 69, 688.
- [56] J. Yang, R. Zhao, Y. Wang, Z. Hu, Y. Wang, A. Zhang, C. Wu, Y. Bai, *Adv. Funct. Mater.* **2023**, 33, 2213510.
- [57] H. Bian, G. Xue, D. Bin, S. Jia, Q. Zhou, H. Lu, X. Meng, *Adv. Funct. Mater.* **2025**, 35, 2417189.
- [58] Q. Jiao, X. Zhai, Z. Sun, W. Wang, S. Liu, H. Ding, W. Chu, M. Zhou, C. Wu, *Adv. Mater.* **2023**, 35, 2300850.
- [59] X. Chen, W. Li, S. Hu, N. G. Akhmedov, D. Reed, X. Li, X. Liu, *Nano Energy* **2022**, 98, 107269.
- [60] H. He, H. Qin, J. Wu, X. Chen, R. Huang, F. Shen, Z. Wu, G. Chen, S. Yin, J. Liu, *Energy Storage Mater.* **2021**, 43, 317.
- [61] C. Li, S. Jin, L. A. Archer, L. F. Nazar, *Joule* **2022**, 6, 1733.
- [62] P. Ruan, S. Liang, B. Lu, H. J. Fan, J. Zhou, *Angew. Chem. Int. Ed.* **2022**, 61, e202200598.
- [63] X. Xie, S. Liang, J. Gao, S. Guo, J. Guo, C. Wang, G. Xu, X. Wu, G. Chen, J. Zhou, *Energy Environ. Sci.* **2020**, 13, 503.
- [64] C. Xu, B. Li, H. Du, F. Kang, *Angew. Chem. Int. Ed.* **2012**, 51, 933.
- [65] J. Zheng, Q. Zhao, T. Tang, J. Yin, C. D. Quilty, G. D. Renderos, X. Liu, Y. Deng, L. Wang, D. C. Bock, C. Jaye, D. Zhang, E. S. Takeuchi, K. J. Takeuchi, A. C. Marschillok, L. A. Archer, *Science* **2019**, 366, 645.
- [66] T. Wang, J. Sun, Y. Hua, B. N. V. Krishna, Q. Xi, W. Ai, J. S. Yu, *Energy Storage Mater.* **2022**, 53, 273.
- [67] Q. Cao, Y. Gao, J. Pu, A. M. Elshahawy, C. Guan, *SmartMat* **2024**, 5, e1194.
- [68] X. Han, S. Mao, Y. Wang, Y. Lu, D. Wang, Y. Sun, Y. Zheng, X. Feng, L. Lu, J. Hua, M. Ouyang, *Nat. Commun.* **2025**, 16, 3699.
- [69] H. Liu, Y. Chen, P.-H. Chien, G. Amouzandeh, D. Hou, E. Truong, I. P. Oyekunle, J. Bhagu, S. W. Holder, H. Xiong, P. L. Gor'kov, J. T. Rosenberg, S. C. Grant, Y. Y. Hu, *Nat. Mater.* **2025**, 24, 581.
- [70] H. Dai, T. Sun, J. Zhou, J. Wang, Z. Chen, G. Zhang, S. Sun, *Nat. Commun.* **2024**, 15, 8577.
- [71] Z. Zhang, J. Wang, H. Qin, B. Zhang, H. Lin, W. Zheng, D. Wang, X. Ji, X. Ou, *ACS Nano* **2024**, 18, 2250.
- [72] J. Zhao, Z. Chen, Z. Chen, Z. Meng, J. Zhang, W. Lv, C. Guo, Z. Lv, S. Huang, Y. Yang, Z. Liu, J. Hui, *ACS Nano* **2025**, 19, 736.
- [73] S. Li, Y. Zhong, J. Huang, G. Lai, L. Li, L. Jiang, X. Xu, B. Lu, Y. Liu, J. Zhou, *Energy Environ. Sci.* **2025**, 18, 2599.
- [74] D. Han, S. Wu, S. Zhang, Y. Deng, C. Cui, L. Zhang, Y. Long, H. Li, Y. Tao, Z. Weng, Q. H. Yang, F. Kang, *Small* **2020**, 16, 2001736.
- [75] J. Hao, X. Li, X. Zeng, D. Li, J. Mao, Z. Guo, *Energy Environ. Sci.* **2020**, 13, 3917.
- [76] Z. Cai, J. Wang, Y. Sun, *eScience* **2023**, 3, 100093.
- [77] Y. Li, Y. Guo, Z. Li, P. Wang, Y. Xie, T. Yi, *Energy Storage Mater.* **2024**, 67, 103300.
- [78] C. Q. Chao, Y. N. Li, Y. Zhao, *Rare Metals* **2024**, 43, 4807.
- [79] J. Zhang, C. You, J. Wang, H. Xu, C. Zhu, S. Guo, W. Zhang, R. Yang, Y. Xu, *Chem. Eng. J.* **2019**, 368, 340.
- [80] C. Mao, Y. Chang, X. Zhao, X. Dong, Y. Geng, N. Zhang, L. Dai, X. Wu, L. Wang, Z. He, *J. Energy Chem.* **2022**, 75, 135.
- [81] X. Qian, Z. Wu, J. Gu, Y. Wang, X. Cheng, J. Zhang, H. Lin, J. Wang, *Chem. Eng. J.* **2025**, 571, 164268.
- [82] S. Iijima, *Nature* **1991**, 354, 56.
- [83] L. Dong, W. Yang, W. Yang, H. Tian, Y. Huang, X. Wang, C. Xu, C. Wang, F. Kang, G. Wang, *Chem. Eng. J.* **2020**, 384, 123355.
- [84] Y. Zhou, J. Xia, J. Di, Z. Sun, L. Zhao, L. Li, Y. Wu, L. Dong, X. Wang, Q. Li, *Adv. Energy Mater.* **2023**, 13, 2203165.
- [85] J. Li, Q. Lin, Z. Zheng, L. Cao, W. Lv, Y. Chen, *ACS Appl. Mater. Interfaces* **2022**, 14, 12323.
- [86] L. He, Q. Zhang, H. Li, S. Liu, T. Cheng, R. Zhang, Y. Wang, P. Zhang, Z. Shi, *Energy Environ. Mater.* **2024**, 7, e12689.
- [87] S. Lai, T. Huang, P. Liu, H. B. Wang, S. C. Yang, X. H. Liu, K. Yang, Q. L. Zhang, J. H. Liu, J. T. Hu, *Rare Metals* **2024**, 43, 1886.
- [88] L. Li, S. Yue, S. Jia, C. Wang, D. Zhang, *Chem. Rec.* **2024**, 24, e202300341.
- [89] Z. Cao, Y. Zhang, Y. Cui, J. Gu, Z. Du, Y. Shi, K. Shen, H. Chen, B. Li, S. Yang, *Energy Environ. Mater.* **2020**, 5, 45.
- [90] A. Xia, X. Pu, Y. Tao, H. Liu, Y. Wang, *Appl. Surf. Sci.* **2019**, 481, 852.
- [91] Q. Wang, J. Zhao, J. Zhang, X. Xue, M. Li, Z. Sui, X. Zhang, W. Zhang, C. Lu, *Adv. Funct. Mater.* **2023**, 33, 2306346.
- [92] Y. Hao, J. Zhou, G. Wei, A. Liu, Y. Zhang, Y. Mei, B. Lu, M. Luo, M. Xie, *ACS Appl. Energy Mater.* **2021**, 4, 6364.
- [93] J. H. Zhou, M. Xie, F. Wu, Y. Mei, Y. T. Hao, R. L. Huang, G. L. Wei, A. N. Liu, L. Li, R. Chen, *Adv. Mater.* **2021**, 33, 2101649.
- [94] X. Yang, J. Lv, C. Cheng, Z. Shi, J. Peng, Z. Chen, X. Lian, W. Li, Y. Zou, Y. Zhao, M. H. Rummeli, S. Dou, J. Sun, *Adv. Sci.* **2023**, 10, 2206077.
- [95] X. Luan, L. Qi, Z. Zheng, Y. Gao, Y. Xue, Y. Li, *Angew. Chem. Int. Ed.* **2023**, 62, e202215968.
- [96] X. Liu, K. Wang, Y. Liu, F. Zhao, J. He, H. Wu, J. Wu, H.-P. Liang, C. Huang, *Carbon Energy* **2023**, 5, e343.
- [97] Z. Xiong, H. Sun, W. Su, W. Jin, H. Liu, Y. Huang, H. Liu, *Small* **2025**, 21, 2502191.
- [98] C. Li, X. Cheng, Y. Zhang, J. Zhu, H. Zhou, Y. Yang, J. Xu, J. Wang, Y. Wang, H. Yu, C. Shen, L. Zhan, L. Ling, *J. Colloid Interface Sci.* **2024**, 671, 505.
- [99] N. Zhang, S. Huang, Z. Yuan, J. Zhu, Z. Zhao, Z. Niu, *Angew. Chem.* **2021**, 133, 2897.
- [100] J. Zhang, L. Pan, L. Jia, J. Dong, C. You, C. Han, N. Tian, X. Cheng, B. Tang, Q. Guan, Y. Zhang, B. Deng, L. Lei, M. Liu, H. Lin, J. Wang, *Nano Lett.* **2025**, 25, 3756.
- [101] C. Liu, Y. Zhu, S. Di, J. He, P. Niu, A. Kelarakis, M. Krysmann, S. Wang, L. Li, *Des. Electron.* **2024**, 2, e29.
- [102] Y. Roh, J. Song, J.-H. Lee, H. Kwon, J. Baek, D. Shin, Y. G. Yoo, S. Ha, W. Kim, K. Ryu, H. T. Kim, *Energy Storage Mater.* **2022**, 51, 777.

- [103] J. Heo, Y. Roh, K. Shin, C. Lee, C. Wang, H. T. Kim, *Energy Storage Mater.* **2024**, 71, 103580.
- [104] J. Jiang, Z. Pan, J. Yuan, J. Shan, C. Chen, S. Li, H. Xu, Y. Chen, Q. Zhuang, Z. Ju, H. Dou, X. Zhang, J. Wang, *Chem. Eng. J.* **2023**, 452, 139335.
- [105] G. Chen, Z. Sang, J. Cheng, S. Tan, Z. Yi, X. Zhang, W. Si, Y. Yin, J. Liang, F. Hou, *Energy Storage Mater.* **2022**, 50, 589.
- [106] Z. Wei, G. Qu, Z. Huang, Y. Wang, D. Li, X. Yang, S. Zhang, A. Chen, Y. Wang, H. Hong, Q. Li, C. Zhi, *Adv. Mater.* **2024**, 36, 2414388.
- [107] Y. Meng, L. Wang, J. Zeng, B. Hu, J. Kang, Y. Zhang, J. Zhang, Z. Zhao, L. Zhang, H. Lu, *Chem. Eng. J.* **2023**, 474, 145987.
- [108] R. Li, Y. Du, Y. Li, Z. He, L. Dai, L. Wang, X. Wu, J. Zhang, J. Yi, *ACS Energy Lett.* **2023**, 8, 457.
- [109] J. Gu, Y. Zhang, Y. Shi, Y. Jin, H. Chen, X. Sun, Y. Wang, L. Zhan, Z. Du, S. Yang, M. Li, *ACS Nano* **2024**, 18, 25966.
- [110] Y. Zhao, S. Guo, M. Chen, B. Lu, X. Zhang, S. Liang, J. Zhou, *Nat. Commun.* **2023**, 14, 7080.
- [111] M. Cui, Y. Xiao, L. Kang, W. Du, Y. Gao, X. Sun, Y. Zhou, X. Li, H. Li, F. Jiang, C. Zhi, *ACS Appl. Energy Mater.* **2019**, 2, 6490.
- [112] Q. Lu, C. Liu, Y. Du, X. Wang, L. Ding, A. Omar, D. Mikhailova, *ACS Appl. Mater. Interfaces* **2021**, 13, 16869.
- [113] M. Liu, K. Yang, Q. Xie, N. Hu, M. Zhang, R. Chen, W. Zhang, J. Zhang, F. Shao, H. He, R. Soni, X. Guo, J. Yang, G. He, F. Pan, L. Yao, T. S. Miller, *Angew. Chem. Int. Ed.* **2025**, 64, e202416047.
- [114] S. B. Wang, Q. Ran, R. Q. Yao, H. Shi, Z. Wen, M. Zhao, X. Y. Lang, Q. Jiang, *Nat. Commun.* **2020**, 11, 1634.
- [115] P. Ruan, X. Chen, L. Qin, Y. Tang, B. Lu, Z. Zeng, S. Liang, J. Zhou, *Adv. Mater.* **2023**, 35, 2300577.
- [116] Y. X. Du, Y. Feng, R. T. Li, Z. Peng, X. Y. Yao, S. Y. Duan, S. D. Liu, S. C. Jun, J. Zhu, L. Dai, Q. Yang, L. Wang, Z. He, *Small* **2024**, 20, 2307848.
- [117] P. Wang, L. Ma, X. Cheng, X. Li, *Int. J. Miner. Metall. Mater.* **2021**, 28, 1112.
- [118] M. Chen, Y. Gong, Y. Zhao, Y. Song, Y. Tang, Z. Zeng, S. Liang, P. Zhou, B. Lu, X. Zhang, J. Zhou, *Natl. Sci. Rev.* **2024**, 11, nwae205.
- [119] R. Zhong, S. Wang, K. He, W. Wang, G. Mo, W. Ma, X. He, W. Liang, J. Li, H. Jin, Z. Ju, Y. Wang, S. Wang, Y. Yuan, *Adv. Mater.* **2025**, 37, 2420166.
- [120] C. B. Deng, X. S. Xie, J. W. Han, Y. Tang, J. W. Gao, C. X. Liu, X. D. Shi, J. Zhou, S. Q. Liang, *Adv. Funct. Mater.* **2020**, 30, 2000599.
- [121] L. Kang, M. Cui, F. Jiang, Y. Gao, H. Luo, J. Liu, W. Liang, C. Zhi, *Adv. Energy Mater.* **2018**, 8, 1801090.
- [122] P. Liang, J. Yi, X. Liu, K. Wu, Z. Wang, J. Cui, Y. Liu, Y. Wang, Y. Xia, J. Zhang, *Adv. Funct. Mater.* **2020**, 30, 1908528.
- [123] S. So, Y. N. Ahn, J. Ko, I. T. Kim, J. Hur, *Energy Storage Mater.* **2022**, 52, 40.
- [124] K. Wu, J. Yi, X. Liu, Y. Sun, J. Cui, Y. Xie, Y. Liu, Y. Xia, J. Zhang, *Nano-Micro Lett.* **2021**, 13, 79.
- [125] J. W. Han, B. K. Park, S. Y. Yang, J. Lee, J. Mun, J. W. Choi, K. J. Kim, *ACS Appl. Mater. Interfaces* **2022**, 14, 48570.
- [126] H. Zhang, P. Wang, C. Yao, S. Chen, K. Cai, F. Shi, *Rare Metals* **2023**, 42, 2516.
- [127] T. Chen, F. Huang, Y. Wang, Y. Yang, H. Tian, J. M. Xue, *Adv. Mater.* **2022**, 9, 2105980.
- [128] H. Yang, F. Liu, B. Chen, X. Cheng, Q. Guan, J. Dong, T. Li, L. Jia, W. Wang, J. Zhang, J. Jia, Y. Zhang, C. Li, Y. Liu, H. Lin, J. Wang, *Chem. Eng. J.* **2025**, 519, 164989.
- [129] S. Zhou, X. Meng, C. Fu, D. Xu, J. Li, Q. He, S. Lin, S. Liang, Z. Chang, A. Pan, *Small* **2023**, 19, 2303457.
- [130] H. Yang, J. Wang, P. Zhang, X. Cheng, Q. Guan, J. Dong, B. Chen, L. Jia, *J. Energy Chem.* **2025**, 100, 693.
- [131] X. Cheng, Y. Zuo, Y. Zhang, X. Zhao, L. Jia, J. Zhang, X. Li, Z. Wu, J. Wang, H. Lin, *Adv. Sci.* **2024**, 11, 2401629.
- [132] Y. Yang, C. Liu, Z. Lv, H. Yang, Y. Zhang, M. Ye, L. Chen, J. Zhao, C. C. Li, *Adv. Mater.* **2021**, 33, 2007388.
- [133] X. Liu, Y. Zhang, L. Wang, R. Diao, T. Li, H. Sun, H. Hu, W. Xing, Z. Yan, *ACS Nano* **2024**, 18, 35325.
- [134] T. Li, X. Li, H. Yang, Y. Zhou, X. Li, M. Su, A. Dou, P. Zhang, X. Wu, A. Naveed, J. Sumner, Y. Liu, *Mater. Today Energy* **2024**, 40, 101513.
- [135] J. Hao, B. Li, X. Li, X. Zeng, S. Zhang, F. Yang, S. Liu, D. Li, C. Wu, Z. Guo, *Adv. Mater.* **2020**, 32, 2003021.
- [136] T. C. Li, Y. V. Lim, X. Xie, X. L. Li, G. Li, D. Fang, Y. Li, Y. S. Ang, L. K. Ang, H. Y. Yang, *Small* **2021**, 17, 2101728.
- [137] J. Zheng, Z. Cao, F. Ming, H. Liang, Z. Qi, W. Liu, C. Xia, C. Chen, L. Cavallo, Z. Wang, H. N. Alshareef, *ACS Energy Lett.* **2022**, 7, 197.
- [138] J. Zhang, C. Han, L. Pan, M. Yang, C. You, Y. Zhang, L. Jia, H. Li, K. Xu, J. Su, H. Lin, J. Wang, *J. Power Sources* **2025**, 640, 236810.
- [139] Z. Jiang, Z. Du, R. Pan, F. Cui, G. Zhang, S. Lei, G. He, K. Yin, L. Sun, *Adv. Energy Mater.* **2024**, 14, 2402150.
- [140] J. Xu, Y. Yang, A. Zhu, Y. Wang, B. Peng, L. Ma, Y. Cao, Y. Wang, *Chem. Eng. J.* **2024**, 487, 150527.
- [141] Z. Zhao, J. Zhao, Z. Hu, J. Li, J. Li, Y. Zhang, C. Wang, G. Cui, *Energy Environ. Sci.* **2019**, 12, 1938.
- [142] J. Hao, X. Li, S. Zhang, F. Yang, X. Zeng, S. Zhang, G. Bo, C. Wang, Z. Guo, *Adv. Funct. Mater.* **2020**, 30, 2001263.
- [143] P. Chen, X. Yuan, Y. Xia, Y. Zhang, L. Fu, L. Liu, N. Yu, Q. Huang, B. Wang, X. Hu, Y. Wu, T. van Ree, *Adv. Sci.* **2021**, 8, 2100309.
- [144] H. Bian, C. Wang, Y. Wang, Y. Ren, Y. Ge, H. Wu, B. Wang, D. Chen, B. Yang, D. Bin, Y. Li, J. Gu, Y. Ma, S. Tang, X. Meng, H. Lu, *Adv. Funct. Mater.* **2024**, 34, 2401760.
- [145] J. Sun, Q. Jian, B. Liu, P. Lin, T. Zhao, *Energy Environ. Mater.* **2024**, 7, e12769.
- [146] H. Yang, Z. Chang, Y. Qiao, H. Deng, X. Mu, P. He, H. Zhou, *Angew. Chem. Int. Ed.* **2020**, 59, 9377.
- [147] X. Liu, F. Yang, W. Xu, Y. Zeng, J. He, X. Lu, *Adv. Sci.* **2020**, 7, 2002173.
- [148] W. Xin, J. Xiao, J. Li, L. Zhang, H. Peng, Z. Yan, Z. Zhu, *Energy Storage Mater.* **2023**, 56, 76.
- [149] C. Zhang, Z. Luo, K. Chen, C. Yan, L. Yi, C. Gong, Y. Cao, F.-S. Ke, *Angew. Chem. Int. Ed.* **2025**, 64, e202500314.
- [150] Y. Zou, Y. Mu, T. Wang, Z. Chen, Z. Shi, W. Guo, T. Shen, Z. Meng, J. Hu, L. Zeng, T. Liu, J. Sun, *Angew. Chem. Int. Ed.* **2025**, 64, e202510080.
- [151] J. Xu, Y. Yang, Q. Dai, Z. Zheng, Y. Cao, Y. Cheng, B. Peng, L. Ma, Y. Wang, *Angew. Chem. Int. Ed.* **2025**, 64, e202423118.
- [152] C. Guo, J. Zhou, Y. Chen, H. Zhuang, Q. Li, J. Li, X. Tian, Y. Zhang, X. Yao, Y. Chen, S. L. Li, Y. Q. Lan, *Angew. Chem. Int. Ed.* **2022**, 61, e202210871.
- [153] K. Zhang, Y. Yuan, G. Wang, F. Chen, L. Ma, C. Wu, J. Liu, B. Zhang, C. Li, H. Liu, C. Lu, X. Li, S. Xi, K. Xie, J. Lin, K. P. Loh, *Energy Environ. Sci.* **2025**, 18, 4210.
- [154] C. Guo, X. Huang, J. Huang, X. Tian, Y. Chen, W. Feng, J. Zhou, Q. Li, Y. Chen, S. L. Li, Y. Q. Lan, *Angew. Chem. Int. Ed.* **2024**, 63, e202403918.
- [155] X. Li, K. P. Loh, *ACS Mater. Lett.* **2019**, 1, 327.
- [156] X. Liang, Y. Tian, Y. Yuan, Y. Kim, *Adv. Mater.* **2021**, 33, 2105647.
- [157] L. Yang, Q. Ma, Y. Yin, D. Luo, Y. Shen, H. Dou, N. Zhu, R. Feng, Y. Kong, A. Yu, B. Cheng, X. Wang, Z. Chen, *Nano Energy* **2023**, 117, 108799.
- [158] Z. Huang, H. Lyu, L. C. Greenburg, Y. Cui, Z. Bao, *Nat. Energy* **2025**, 10, 2058.
- [159] J. Ming, J. Guo, C. Xia, W. Wang, H. N. Alshareef, *Mater. Sci. Eng. R. Rep.* **2019**, 135, 58.
- [160] Z. Peng, X. Shen, B. Li, J. Cheng, Z. He, Z. Sun, B. Li, Z. Zhang, Z. Zhuang, X. Wu, L. Dai, L. Wang, G. He, Q. Zhang, *Prog. Mater. Sci.* **2025**, 152, 101453.
- [161] X. Zhang, L. Zhang, X. Jia, W. Song, Y. Liu, *Nano-Micro Lett.* **2024**, 16, 75.